SPIRE Bolometer Array Noise Performance

Bernhard Schulz, Nanyao Lu, Kevin Xu, Lijun Zhang (IPAC/Caltech),
Jamie Bock, C. Darren Dowell, Hien Nguyen (JPL), Glenn Laurent (U. Colorado)

Contents

1. Introduction and Scope

The noise performance of the SPIRE detector arrays was analyzed during every test campaign starting from the assembly level tests at JPL with BoDAC and continuing during the 5 instrument test campaigns at RAL. Much experience was gathered along the way, however only the last test campaign PFM 5, which was performed in a dark test environment, gave the highest quality measurements and the most complete dataset for this task.

In the following we will give a summary of the operational status of the detector channels, and describe the general way we processed data for this analysis. As we learned that temperature variations have the strongest influence on signal stability, we discuss 1/f noise and removal of its temperature component first before continuing with basic white noise and microphonics.

2. Broken, Noisy and Peculiar Channels

In the following the detector channels are designated by their QLA channel number in FULL mode, and by their JPL detector names. The prefixes PSW, PMW, PLW, identify the photometer arrays, SSW, and SLW stand for the spectrometer detector arrays. PTC identifies the thermistor channels of the temperature control unit for the photometer arrays.

Tables 2-1 to 2-2 show the history of peculiar detector channels that showed any anomaly like excessive noise, no signal, or unusual load curves during the test campaign at JPL at assembly level in the BoDAC facility, and during the last 3 PFM test campaigns (PFM 3-5) at RAL, where all channels were connected. The meaning of the various entries is explained at the end of Table 1-2. The last column indicates individual identifications of failure modes that resulted mostly from a physical check of the test cryo-harness between the PFM 4 and 5 test campaigns. At that occasion a high voltage check of the harness effected a "healing" of a number of channels by burning away the respective shorts.

Most non-operational channels were due to harness problems. Since the test cryo-harness will be replaced by the one of the spacecraft after integration, these channels can potentially be recovered. The number of channels per array that were bad in the last test campaign, but were still functional during the BoDAC test campaign on assembly level, are 3, 6, 0, 0, 2 respectively for arrays PSW, PMW, PLW, SSW, and SLW. They may in principle be recovered with the satellite harness. There are only very few dead channels due to broken bolometers in the BDAs or broken LIA channels that will likely remain unusable during the mission. We also include in this count extremely noisy or intermittent channels. We find 5, 1, 0, 2, 2 of these unrecoverable channels respectively for arrays PSW, PMW, PLW, SSW, and SLW.

We note that channels, PS_F14(83), PS_H16(93) and PS_E9(104) were not measured in BoDAC, but are nevertheless functional on instrument level. The channels SS_DK1(6), SS_B3(7), SS_D3(13), SS_D1(15), SS_E1(18) were found noisy in BoDAC, but seem not to be peculiar in the instrument tests.

Channel PS_G11(144) is intermittent, as it showed strong noise in the early PFM 3 tests, was fine later during PFM 4 and became again very noisy in PFM 5. From a PCAL measurement performed June 21, 2006 11:39, we found two more pixels with long optical time constants. These are PS_A11(22) and PM_A13(193).

Channels that deviate from the median noise by more than $\sqrt{2}$ are listed as "Noisy". Channels that exhibit noise levels of more than a factor of 2 more than the median are listed as "Very Noisy".

A full list of all detector channels with noise values under optimum conditions can be found in Tables 7-1 and 7-2. Channels that are considered permanently defunct are greyed out. Channels with any history of peculiarities during the test campaigns are marked with a bold font.

Table 2-1: History of peculiar channels during SPIRE test campaigns for the PSW array. BoDAC indicates the status of detector channels during the assembly level tests at JPL. The columns PFM 3 – 5 indicate channel states during the last three PFM test campaigns. The last column shows individual failure modes.

channel	BoDAC	PFM3	PFM4	PFM5	failure mode
PSW_A10	slow 41.4ms	short/open	noop	inactive	Bad contact S-?
PSW_A11	slow 15.8ms			very slow	
PSW_A12			offset		
PSW_A13	slow 360ms			very slow	
PSW_A14		noisy			
PSW_A8			noisy		
PSW_B3			noop	bad LC	low gain, LIA problem ????
PSW_B5	noisy	noisy	noisy		
PSW_B12		noisy	sl. noisy		
PSW_C11		noisy			
PSW_C12	dead	dead	dead	bad LC	BDA dead
PSW_D11	slow 45.4ms				
PSW_D12			offset		
PSW_D14		noisy	noisy/interm		
PSW_DP2		noisy			
PSW_F8	noisy		noop	bad LC	Broken S+
PSW_F9			slnoisy	LC feature	Noisy JFET
PSW_F11			noisy		
PSW_G8	m. noisy	dead	dead	bad LC	BDA dead post PFM2
PSW_G11	interm		noisy	v. noisy, LC feature	very noisy
PSW_G13		noisy			
PSW_H9		short/open			
PSW_J6		short/open	noop		Short to ground S+ (PFM4)
PSW_J7	interm	interm	noisy/interm	very noisy	very noisy

channel	BoDAC	PFM3	PFM4	PFM5	failure mode
PMW_A8		noisy			
PMW_A11		noisy			
PWM_A13				very slow	
PMW_B1		noisy			
PMW_B6		short/open	noop	bad LC	Broken S+
PMW_B11			noisy	noisy	
PMW_C8		short/open	noop	inactive	Broken S-
PMW_C9			offset		
PMW_D6				noisy	
PMW_D9			noisy		
PMW_DP1			noop		Broken S- (PFM4)
PMW_E4		noisy	noisy	noisy	
PMW_E5		noisy	noisy	noisy	
PMW_F2		noisy			
PMW_F5		noisy	noisy	noisy	
PMW_F6		noisy		noisy	
PMW_F7		short/open	swap	bad LC	wiring swap
PMW_G6		noisy	noisy	very noisy	very noisy
PMW_G7		noisy			
PMW_G9		short/open	noop	bad LC	Short to ground S+
PMW_G11			noop	bad LC	Bad contact S+?
PMW_T2		short/open	noop	inactive	Broken S-

Table 2-2: Continuation of Table 2-1 and legend.

channel	BoDAC	PFM3	PFM4	PFM5	failure mode
PLW_A2		short/open	noop		
PLW_A6		noisy	noisy/offset		
PLW_B4			noop		
PLW_C9		noisy	noisy		
PLW_DP1			noop		Broken S+ (PFM4)
PLW_E2			noop		
PLW_T2			offset		
SSW_A2		noisy			
SSW_A3		noisy	slnoisy		JFET Vss (PFM4)
SSW_D5	dead	dead	dead	bad LC	BDA dead
SSW_D7			noop		Bad contact S+ (PFM4)
SSW_E3		noisy			
SSW_F4	noisy		micro/slnoisy	very noisy	JFET Vss noisy (PFM4)
SLW_A3		noisy			
SLW_B3		short/open	noop	inactive	Broken S+
SLW_C1		noisy			
SLW_C2		short/open	noop	inactive	Broken S+
SLW_D2		noisy			
SLW_DP2	dead	dead	dead	inactive	BDA dead
SLW_E2		noisy			
SLW_T2		noisy			
PTC3		short/open			cryoharness wiring swap

Colours	Meaning
	channel likely to be lost
	problem with test cryoharness
	harness problem fixed after PFM4, or suspected failure

Remark	Meaning
dead	channel not operational
slnoisy	slightly noisy more than sqrt(2) times of median
noisy	detector noise more than 2 times median
very noisy	detector noise
short/open	cabling problem
noop	channel not operational
inactive	signal shows single value only
LC feature	small kink in Load Curve
bad LC	unusual shape of Load Curve

3. 1/f Noise and Temperature Instabilities

3.1 Introduction and Scope

This chapter summarizes the results of a study on the temperature drift correction to observational data taken by the SPIRE bolometer detectors. Such a correction will minimize the low frequency 1/f noise. Among different SPIRE observation modes, the 1/f noise affects most significantly the scan mapping mode in the photometer AOT. Therefore we will concentrate on the photometer arrays.[1]

3.2 Data and Basic Processing

Two data sets are analyzed in this study. Both are taken from the noise stability test campaign in PFM 5. The parameters of the tests yielding these data sets are listed in Table 3-1 below. These are dark tests with minimal optical loading. The temperature stabilization circuit (PTC) was not active during these measurements.

Table 3-1: List of test data considered for this analysis.

OBSID	Date	Start	End	BiasFreq	BiasAmp	Measurement Type
3001233C	24-Feb-07	04:08	10:25	131.1 Hz	28.4 mV	Photometer noise stability. No PTC.
30012342	24-Feb-07	23:05	05:21	90.42 Hz	17.2 mV	Photometer noise stability. No PTC.

Each of the two data sets contains about 6 hours of test data. In this analysis, only 1 hour of data in each set are utilized. The data are retrieved from database PFM5_test1 using the *QLA Export Tool*. The basic data processing, including data conversion, offset adding, derivation of the power spectra, determination of the white noise plateau and the 1/f knee, is carried out using the same software package as described in detail in the following chapter about white noise.

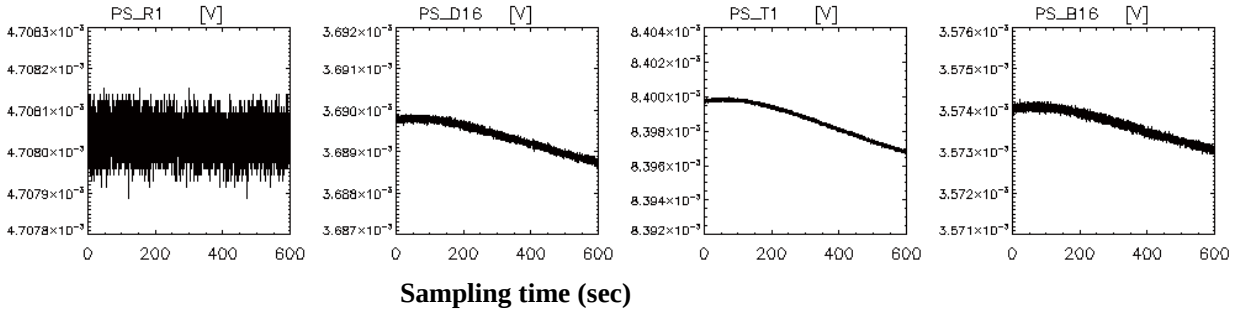

Figure 3-1: Example of long term signal drift, taken from the test 3001233C.

3.3 Effects of Temperature Drift

In the PFM 5 dark noise tests, we see ubiquitously long term signal drifts in detector channels, with time scales longer than a few minutes. The scale of the signal drift is on the order of 0.1%, though occasionally it can be as high as ~0.5 % (see chapter on white noise). An example, taken from the test 3001233C, is

[1] The correction can however also be applied to spectrometer data. This was used for the purpose of extracting white noise levels from the spectrometer data.

shown in Fig. 3-1. It appears that the signal of the resistor channel PS_R1 is flat, indicating that the drift is not due to the amplifier electronics chain. *The signal drift of the detector channels correlates very well with that of the thermistor channel PS_T1, suggesting it is caused mainly by the temperature drift of the thermal bath.* This is the major source of the low frequency 1/f noise of the SPIRE bolometer arrays, as discussed in Section 6 of B. Schulz's report on SPIRE Bolometer Array Noise Performance during the PFM 1, 2, and 3 Test Campaigns. In Fig. 3-2, we show the signal time lines of the thermistor channel PS_T1 in 3001233C and 30012342, respectively. The amplitude of the long term fluctuation is of the order of 0.06% in both cases. Note that in 3001233C, there is a relatively sharp turn at t ~ 3200s.

PS_T1 in 3001233C

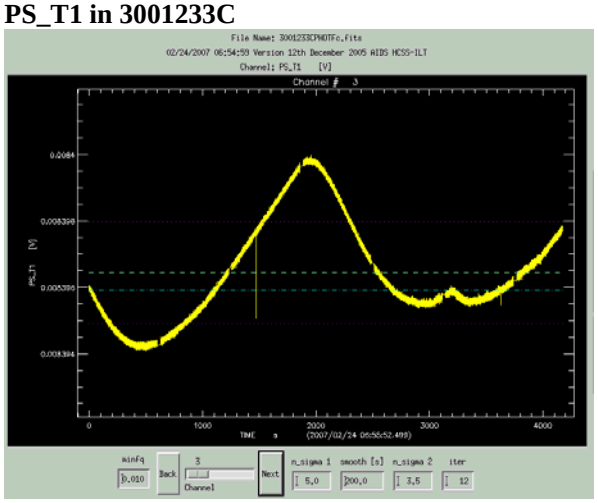

PS_T1 in 30012342

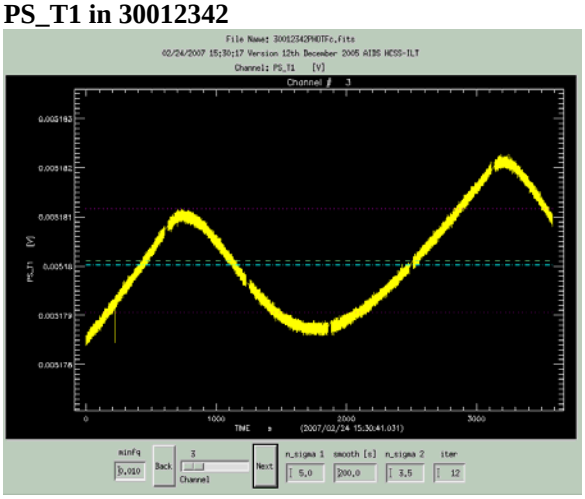

Figure 3-2: The signal time lines of the thermistor channel PS_T1 in 3001233C and 30012342. The amplitude of the long term fluctuation is of the order of 0.06% in both cases.

3.4 Correction of Temperature Drift – An Empirical Approach

There is a nearly perfect linear correlation between signal drift of the detector channels and that of the thermistor channels. Some examples are shown in Fig. 3-3.

The very tight linear correlation suggests by itself an empirical approach for the correction of the effects of the temperature drift. In this approach, we bypass the detector model, and assume (1) the drift of the bath temperature is proportional to the drift of the thermistor signals, and (2) the tight detector/thermistor correlation specifies the temperature dependence of the detector signal. Obviously, these assumptions are valid only when the amplitude of the signal drift is much less than the signal itself (small perturbation condition), which generally applies in our cases.

The procedure for the temperature drift correction in this empirical approach consists of the following steps:

I) First of all, a definition for the signal drift is in order. For a given detector in a given array, the signal drift is:

$$\text{drift} = \text{signal} - \text{mean}(\text{signal}) \qquad (1)$$

where signal is the time ordered signal data (in V) of the detector, mean is the statistical mean over the time line.

II) Fit the time ordered signal drift of each thermistor (T1 or T2) by a smooth function ($f\_{T1}(t)$ or $f\_{T2}(t)$). The smoothing is to get rid of the higher frequency noise in the thermistor signal that is not caused by the temperature variations. In this analysis, three function forms are explored. They are: (1) 3rd order polynomial, (2) SPLINE fit, (3) moving median. We also tested 3 different widths of the time window for smoothing: 0.3 sec, 1 sec and 5 sec. The five algorithms explored in this approach are listed in Table 3-2.

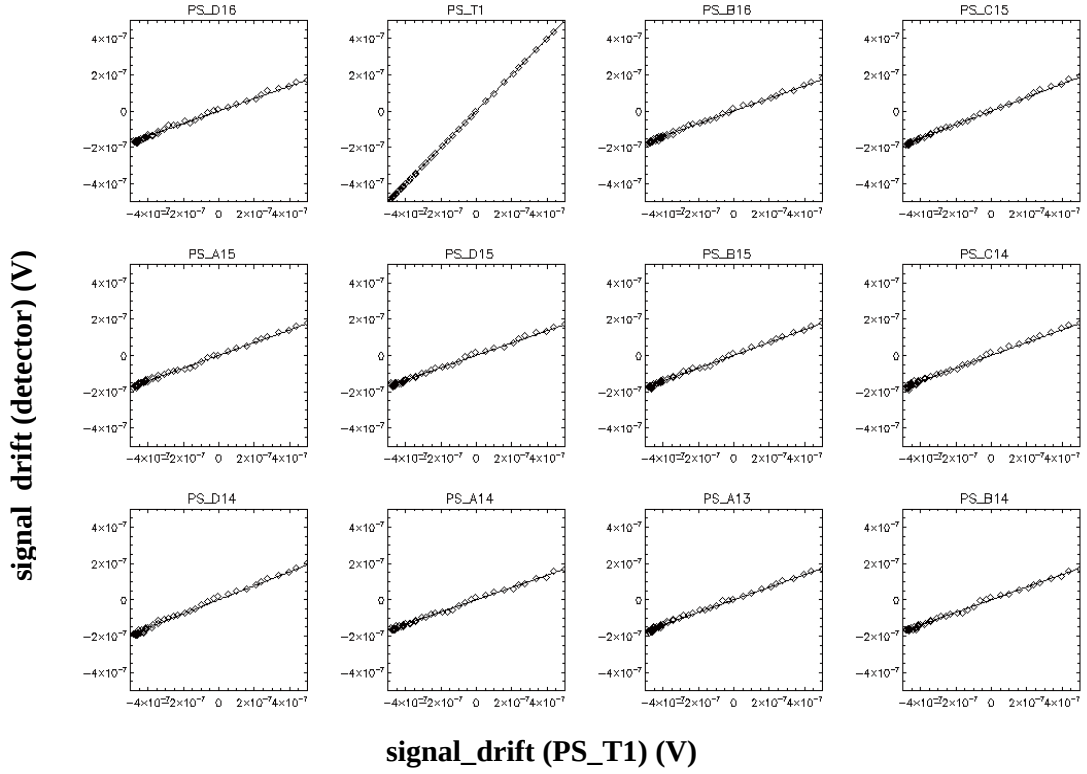

Figure 3-3: Examples of correlation between signal drift of detector channels and that of thermistor PS_T1.

III) Determine the temperature dependence of the detector signal drift. Here we also explored 3 different methods:

i) **Method T1**: Assume the bath temperature drift is proportional to the signal drift of the thermistor T1 only. The detector signal drift due to the bath temperature drift can be specified by the linear regression:

$$\mathrm{Drift}_{\mathrm{detector}}(\mathrm{T1}) = a_0 + a_{\mathrm{T1}} \times \mathrm{drift}_{\mathrm{T1}} \qquad (2)$$

ii) **Method T1+T2**: Assume the bath temperature drift is proportional to the sum of the signal drifts of both, T1 and T2:

$$\mathrm{Drift}_{\mathrm{detector}}(T1+T2) = b_0 + b_{T1+T2} \times (\mathrm{drift}_{T1} + \mathrm{drift}_{T2}) \qquad (3)$$

Table 3-2: List of algorithms to fit the thermistor signal by a smooth function.

Name	Function form	Δt	Note
CUBIC	3rd order polynomial	5.0	Fit to Time ordered Data (ToD) of 600 sec
SPLIN5	SPLINE	5.0	SPLINE fit to ToD smoothed to Δt=5.0 sec
SPLIN1	SPLINE	1.0	SPLINE fit to ToD smoothed to Δt=1.0 sec
MMD10	Moving Median	1.0	Moving median of ToD with tine window Δt=1.0 sec
MMD03	Moving Median	0.3	Moving median of ToD with time window Δt=0.3 sec

iii) **Method T1&T2**: Assume the temperature drifts measured with each thermistor have different influence, depending on detector pixel. Derive the optimal combination of the T1 and T2 dependence by minimizing the χ^2 of $[\mathrm{drift}_{\mathrm{detector}} - \mathrm{Drift}_{\mathrm{detector}}(T1,T2)]$, where

$$\mathrm{Drift}_{\mathrm{detector}}(T1,T2) = c_0 + c_{T1} \times \mathrm{drift}_{T1} + c_{T2} \times \mathrm{drift}_{T2} \qquad (4)$$

Note that a_0, b_0 or c_0 shall be close to zero by definition. And PM_T2 is non-operational in PFM 5, so $c_{T2} = 0$ for all PMW channels.

IV) Depending on which method is used, replace drift_{T1} and drift_{T2} in EQ(2), EQ(3) or EQ(4) by the smooth functions $f\_{T1}(t)$ and $f\_{T2}(t)$. Subtract the resulting signal drift due to temperature drift, and obtain the corrected detector signal:

$$\mathrm{signal}_{\mathrm{corrected}} = \mathrm{signal} - \mathrm{Drift}_{\mathrm{detector}} \qquad (5)$$

3.5 Metrics

Typically the 1/f noise component is characterized by the frequency, where white noise and 1/f noise are equal. For a perfect 1/f noise spectrum, this is where the noise reaches √2 times the white noise level. After correcting for temperature drift, the power spectrum still shows the white noise plateau and high frequency roll-off, however, the low frequency spectrum rises shallower than with a 1/f dependency towards lower frequencies and appears more irregular. This and the fact that the power spectra become noisier towards the lower frequencies, affects our determination of 1/f knee frequencies, especially below 50 mHz for this dataset. As a more robust indicator we chose the ratio between the median over a defined interval in the low frequency power spectrum (3…30 mHz) and the white noise level (median over 0.5..2.0 Hz). For comparison, we still fit the corrected data with a 1/f law and derive the 'knee' using the same procedure as applied to noise data without temperature correction. There is a good correlation between the ratio and the 1/f knee, which could indicate that a power law is still a valid description for the low frequency noise; however this will need further investigation with larger datasets over longer time intervals. For now the 1/f knee values have to be treated with caution.

3.6 Results

In Table 3-3, 3-4 and 3-5, results of temperature drift corrections using the 3 different methods (T1, T1+T2 and T1&T2) and 5 different fitting functions are compared with each other. The medians are derived from values of all detector channels (resistors and thermistors are excluded), except for the dead and very noisy ones. In addition to the bad channels listed in Tables 2-1 and 2-2, channels PS_B3(61), PS_B5(54), PM_B11(200), and PL_A1(166) appear to be very noisy or disconnected during the tests analyzed here and are excluded.

Table 3-3. Results of temperature drift correction algorithms using the T1 method. The medians are over all detector channels except for the dead and very noisy ones. Median white noise is taken over an interval of 0.5 - 2 Hz; the median low frequency noise is taken over the interval 3 – 30 mHz.

	Test1 (3001233C)				Test2 (30012342)			
algorithm	**med. white noise**	**med. 1/f knee**	**med. low frequ. noise**	**med.ratio**	**med. white noise**	**med. 1/f knee**	**med. low frequ. noise**	**med.ratio**
	nV/√Hz	mHz	nV/√Hz		nV/√Hz	mHz	nV/√Hz	
CUBIC	14.2	25.8	40.30	2.80	14.5	20.3	33.6	2.30
SPLIN5	14.2	21.8	33.78	2.36	14.5	21.5	34.6	2.34
SPLIN1	14.2	20.8	32.88	2.30	14.6	21.5	34.9	2.39
MMD10	14.4	20.6	32.74	2.26	14.6	22.2	36.3	2.43
MMD03	15.0	19.8	32.90	2.19	16.3	19.3	35.6	2.17

Table 3-4. Results of temperature drift correction algorithms using the T1+T2 method

	Test1 (3001233C)				Test2 (30012342)			
algorithm	**med. white noise**	**med. 1/f knee**	**med. low frequ. noise**	**med.ratio**	**med. white noise**	**med. 1/f knee**	**med. low frequ. noise**	**med.ratio**
	nV/√Hz	mHz	nV/√Hz		nV/√Hz	mHz	nV/√Hz	
CUBIC	14.2	25.4	39.76	2.76	14.5	20.1	33.1	2.26
SPLIN5	14.2	22.0	34.26	2.41	14.5	21.8	35.7	2.43
SPLIN1	14.2	21.4	33.58	2.33	14.5	22.0	35.8	2.43
MMD10	14.3	21.2	33.54	2.13	14.7	21.8	36.0	2.42
MMD03	14.7	20.8	33.72	2.27	15.7	20.2	36.0	2.27

Table 3-5: Results of temperature drift correction algorithms using the T1&T2 method.

	Test1 (3001233C)				Test2 (30012342)			
algorithm	**med. white noise**	**med. 1/f knee**	**med. low frequ. noise**	**med.ratio**	**med. white noise**	**med. 1/f knee**	**med. low frequ. noise**	**med.ratio**
	nV/√Hz	mHz	nV/√Hz		nV/√Hz	mHz	nV/√Hz	
CUBIC	14.2	25.4	39.62	2.76	14.5	20.2	33.2	2.27
SPLN5	14.2	20.8	32.78	2.30	14.5	20.2	33.6	2.29
SPLN1	14.2	20.4	32.18	2.25	14.6	20.8	34.1	2.33
MMD10	14.3	20.0	32.02	2.24	14.7	21.4	35.1	2.37
MMD03	14.7	20.0	32.58	2.21	15.7	20.0	35.1	2.21

It appears that the T1&T2 method yields the best results and the T1+T2 method the worst. Judging from the median residual low frequency noise, the difference between the methods is only ~4%. However, for individual detector channels, the difference can be as large as 20%. Among the 5 algorithms studied here, CUBIC gives a significantly higher median 1/f knee for the data of test 3001233C. This is because it cannot handle temperature drift properly on a time scale shorter than a few tens of seconds, and in 3001233C there is a significant fluctuation on such a time scale (Fig. 3-2). On the other hand, the CUBIC correction results in the lowest residual low frequency noise for the data in test 30012342, which has no sharp temperature fluctuations. The moving median algorithms MMD03 gives relatively high white noise. This is because the electronic noise in the thermistor data is not sufficiently suppressed in this algorithm, and is added to the detector data during the temperature drift subtraction. The two algorithms based on the SPLINE fit functions give the most robust performance.

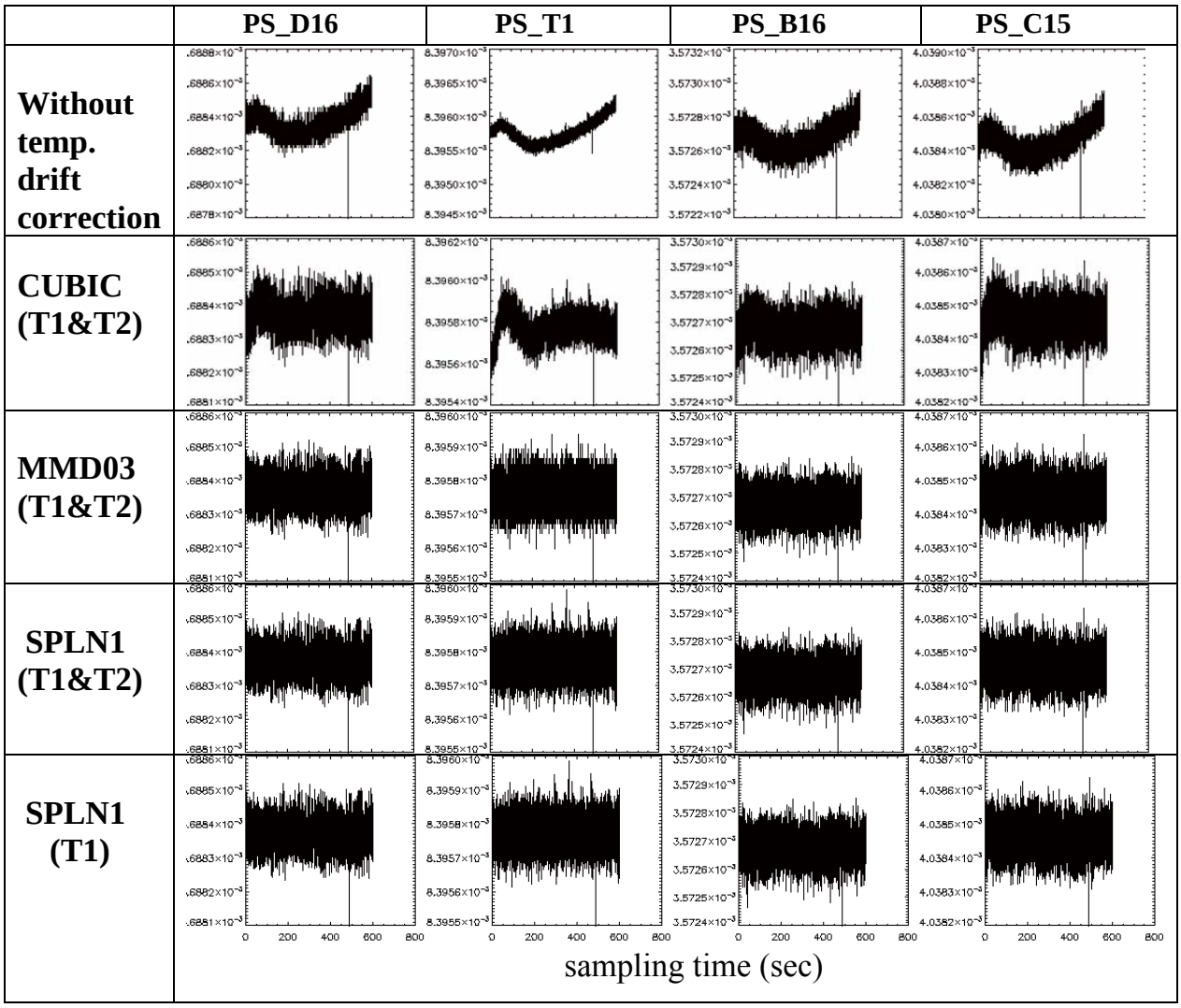

Figure 3-4: Detector signals before and after the temperature drift correction. The data are taken from test 3001233C.

In Fig.3-4, examples of detector signals before and after the temperature correction are shown. The sampling time period includes the moment when the relatively sharp turn in the thermistor signal occurred in the test 3001233C. Time lines of 4 channels are shown, including 3 detector channels (PS_D16,

PS_B16 and PS_C15) and 1 thermistor channel (PS_T1). Results of 4 temperature drift correction algorithms are displayed, including 3 based on the T1&T2 method and 1 using the T1 method. The CUBIC algorithm is problematic, leaving the sharp upturn in the PS_T1 time line uncorrected. The difference among the other 3 algorithms is rather subtle.

In Fig.3-5, the power spectra of the signal data shown in Fig.3-4 are plotted. The left-most vertical dashed lines mark the frequency of the best-fit 1/f knee (when no 1/f noise knee is detected, no such line is shown). For the uncorrected data, the 1/f knee is always > 100 mHz. The 1/f knee of data after the correction using the CUBIC algorithm is still high, between 50 and 100 Hz. Except for the PS_T1 channel, the power spectra obtained using the other 3 algorithms are very similar. For PS_T1, the algorithm MMD03 produced a sharp cut-off below ~3 Hz because of the 0.3 sec median (high-pass) filter. We note that the SPLN1 algorithm with T1&T1 or T1 only shows a sharp drop of the noise power below 400 mHz as the thermistor signal is corrected by its own variations. Note also that in most of the cases, the spectra of the residual low frequency noise (< 30 mHz) are not in the 1/f form. They look more like an elevated plateau above the white noise level, with the elevation at about a factor of 2.

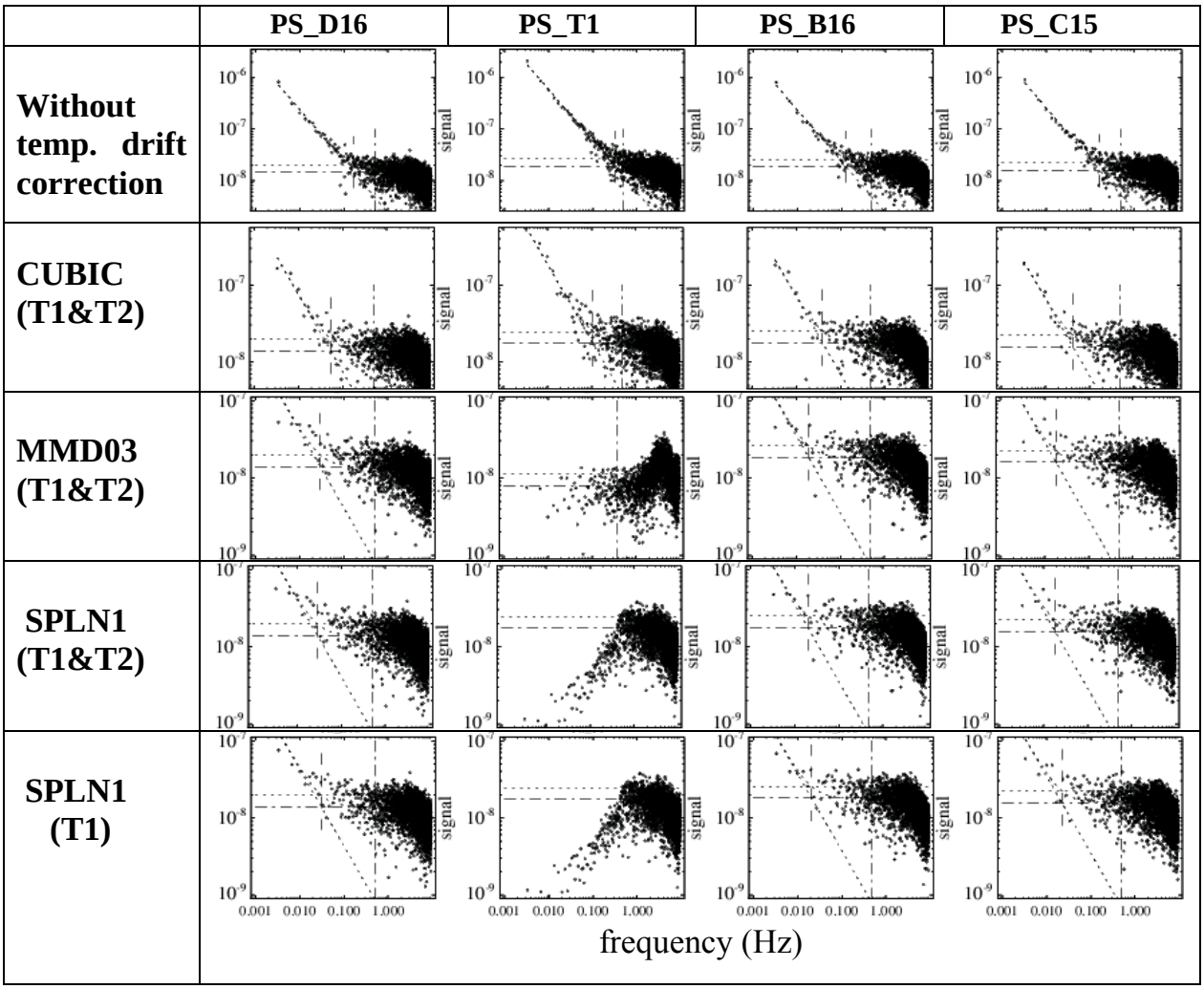

Figure 3-5: Power spectra of the signal data shown in Fig.3-4 are plotted. The vertical dashed lines mark the frequency of the best fit 1/f knee. When data do not have 1/f noise, no such line is shown.

To see whether the still elevated low-frequency noise in the corrected data is due to some remaining temperature dependence, we plot the residual signal drift of the data after the temperature drift correction using the SPLN1 algorithm (T1 method) in Fig. 3-6 against the uncorrected signal drift of the PS_T1(3) channel. There is no evidence for any residual temperature dependence in the corrected data. It is unlikely that the residual low frequency noise is still due to temperature drift.

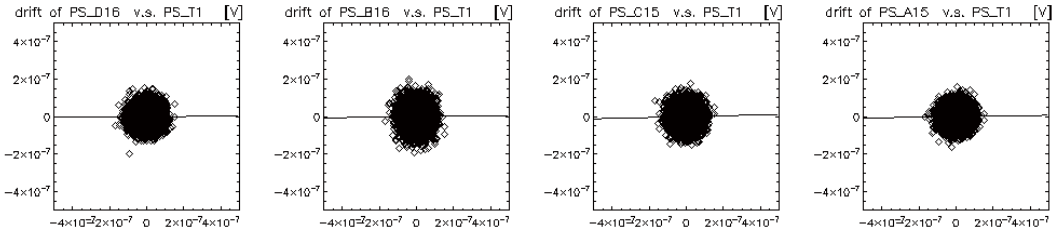

Figure 3-6: Examples of cross correlation between detector signal drifts after the temperature drift correction (SPLN1/T1 algorithm) and the uncorrected PS_T1 signal drift.

Nevertheless, the residual low frequency noise may be further reduced by subtracting correlated noise among detectors in the same array. This has been tested in an exploratory study. In this study the correlated noise in the temperature drift corrected time line, derived using the SPLN1/T1&T2 algorithm, of the test 3001233C, was analyzed and corrected using a Principal Component Analysis (PCA) algorithm. An example of the results is shown in Fig.3-7, which compares the mean power spectra (averaged over all good pixels) of the PSW array before and after the PCA correction. Indeed the low frequency noise below ~0.05 Hz is further reduced. But the improvement is only marginal. This is actually true for the temperature drift corrected data in general. This result confirms that for the SPIRE detector arrays, the correlated 1/f noise is predominantly due to the temperature drift.

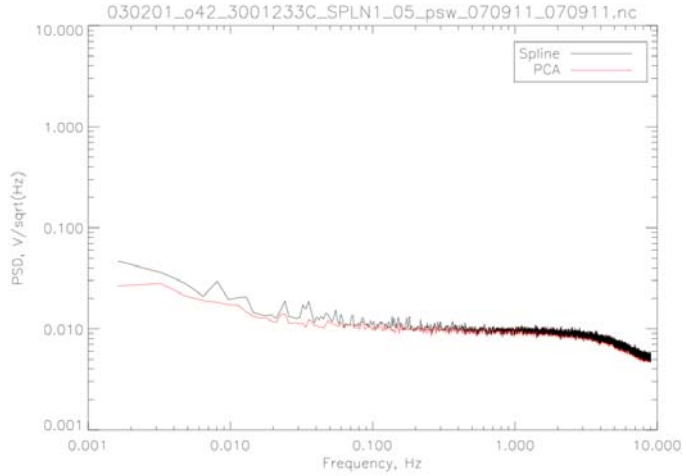

Figure 3-7: Comparison of mean power spectra (averaged over all good pixels) of the PSW array before and after the PCA correction. The data are taken from the temperature drift corrected time line, derived using the SPLN1/T1&T2 algorithm, of test 3001233C. The black curve is the mean noise power spectrum before the PCA correction, and the red curve the mean noise power spectrum after the PCA correction.

3.7 Theoretical Approach Based on Bolometer Model

In principle, the bath temperature dependence of the detector signals can be calculated and then removed using the detector model. To test this, we applied the theoretical detector model according to Mather, adopting the detector parameters determined at assembly level with BoDAC, to convert the detector signal in test 3001233C into optical in-band power. For this test we determined the bath temperature from the thermistor T1 in each array, and applied a box-car smoothing to remove high frequency noise. The same analysis as used before on the detector signal to derive the 1/f knee, and the ratio between low frequency noise (<30 mHz) and the white noise, was applied to the optical power. In Table 3-6, the medians of these values are compared with those of the uncorrected signal and those of the signals after the SPLN1 (T1&T2) correction. Both the model correction and the SPLN1 (T1&T2) correction reduce the low frequency noise by about an order of magnitude. However, the theoretical approach is less effective than the empirical approach. In particular, for the PSW array, the residual low frequency noise after the model correction is significantly higher (> 50%) than the SPLN1 (T1&T2) correction, as measured either by the 1/f knee or by the low-frequency/white-noise ratio. This result, however, can not be regarded as final yet as we are still using model parameters derived with an experimental setup with DC-bias for a correction of data from an AC-bias experiment. We have also not yet paid any special attention to the second thermistor signal and smoothing methods as described above. Residual systematic uncertainties will need to be removed first by deriving the model parameters from the PFM 5 dataset, which potentially could reduce the gap between both methods further.

Table 3-6: Medians of the 1/f knee and of the ratio between low frequency noise (<30 mHz) and white noise. Comparisons between uncorrected data, model corrected data, and data after the SPLN1 (T1&T2) correction.

	total		PSW		PMW		PLW	
	med. 1/f knee	med. ratio	med. 1/f knee	med. ratio	med. 1/f knee	med. ratio	med. 1/f knee	med. ratio
	(mHz)		(mHz)		(mHz)		(mHz)	
Uncorrected	290.6	29.9	298.8	30.7	281.6	28.7	275.2	28.6
detector model	28.0	2.86	34.6	3.52	21.6	2.38	26.4	2.75
SPLN1 (T1&T2)	20.4	2.25	20.8	2.26	19.2	2.17	21.6	2.33

3.8 Dependence of Detector/Thermistor Correlation on V_{bias} , f_{bias} , and T_{sub}

Using the same PFM 5 noise test datasets (23 tests, 9 for photometer and 14 for spectrometer) as analyzed in the next chapter, we studied the dependence of the detector/thermistor correlation on three different testing parameters: (1) the bias voltage V_{bias}, (2) the bias frequency f_{bias} , and (3) the sub-K temperature $T_{sub.}$ In Fig.3-8 we plot the median slope (over all detector channels) of the linear regression of the signal drift over that of T1 against V_{bias}. The dependence on V_{bias} is strong. However, there is no evidence for any significant dependence on f_{bias} or $T_{sub.}$

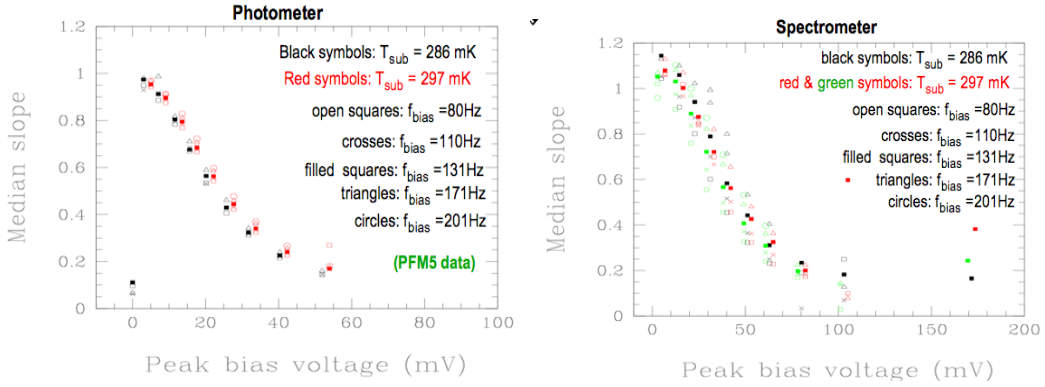

Figure 3-8: Dependence of the slope of the linear regression of the detector signal drift over that of the thermistor. The median is over all detector channels. The left plot is for the photometer arrays, and the right for the spectrometer arrays. The data is taken from the PFM 5 noise test data discussed in the next chapter.

3.9 Summary and Conclusions for Temperature Drifts

1. The long term signal drift seen ubiquitously in SPIRE bolometer data is due to the temperature drift of the thermal bath. It is the major source of the low frequency 1/f noise.
2. The correlations between detector signal drifts and thermistor signal drifts are very tight and linear, suggesting an empirical approach for the temperature drift correction.
3. Fifteen different algorithms in this empirical approach have been studied. They differ in two aspects: (1) the way how the bath temperature is specified using signals of the two thermistors T1 and T2; and (2) the form of the fitting function of thermistor signal timelines.
4. All of these algorithms can reduce the low frequency noise by more than a factor of 10. The difference between them, in terms of median low frequency (< 30 mHz) noise power in the corrected data, is < 30%. The algorithms SLPN1(T1&T2) and SPLN5(T1&T2) give the most robust performance.
5. The residual low frequency noise in the corrected data is generally not anymore of the 1/f form. The low frequency power spectrum rises above the white noise plateau shallower than a 1/f spectrum, and it is not clear whether a power spectrum is still a good model description. If we ignore this, and determine the 1/f knee using the same procedure as is applied to the uncorrected data, the median 1/f knee for data after the temperature drift correction (e.g. using the SPLN1(T1&T2) algorithm) is ~20 mHz.
6. No correlation is found between the detector signals and the thermistor signals after the correction. Therefore the still elevated residual low frequency noise is not due to any remaining temperature dependence in the corrected data.
7. A theoretical approach has also been explored and the preliminary results go into the same direction but have not yet reached the performance of the empirical algorithms (e.g. SPLN1(T1&T2)). More investigation is needed as the current parameter set and temperature filtering are not optimized yet.
8. In a large set of noise tests data spanning different bias voltages $V_{bias,}$ bias frequencies f_{bias} and fridge temperatures T_{sub} (SUBKTEMP), we found a strong dependence of the detector/thermistor correlation on V_{bias}, but no evidence for any significant dependence on f_{bias} or $T_{sub.}$

4. White Noise

4.1 Introduction

During the PFM 5 testing campaign, which was the first fully dark campaign for the SPIRE PFM instrument, the noise measurements were carried out at two temperatures of the He^3 fridge, T_subk = 286 and 297mK, under a range of bias frequencies (f_bias = 80-201 Hz for the photometer and 100-205 Hz for the spectrometer) and peak bias voltages (V_bias = 0-86.6 mV for the photometer and 4.8-171.5 mV for the spectrometer). The goals of these tests were to assess detector noise behaviour as a function of those three parameters, to compare them with model predictions, and to optimize the bias settings for minimum overall detector noise.

The power spectra of the SPIRE bolometer channels show three distinct noise components (e.g., Schulz et al 2006): (a) a high frequency roll-off at the lowpass limits of photometer and spectrometer at 5 or 25 Hz respectively, (b) a relatively flat white noise plateau, and (c) a 1/f noise component that rises above the white noise level at frequencies < 0.1 Hz. The frequency where the white noise and 1/f noise components equal each other is conventionally called the 1/f knee frequency. As shown in the previous chapter, (c) is usually insignificant at frequencies > 0.03-0.05 Hz after any temperature-based drift in time is removed from the detector signal. In this chapter we concentrate on the white noise component (b), which is measured after empirically removing any significant temperature-based drift in the measured signal.

Table 4-1: List of Photometer Dark Noise Measurements.

OBSID	Date	T_subk (K)	f_bias (Hz)	V_bias (mV)
30012150	02/13/2007	0.286	80.37	0 – 86 (12 settings)
30012151	02/13/2007	0.286	110.35	0 – 86 (12 settings)
30012152	02/13/2007	0.286	131.08	0 – 86 (12 settings)
30012153	02/13/2007	0.286	171.33	0 – 86 (12 settings)
3001226D	02/19/2007	0.297	80.37	3 – 86 (11 settings)
3001226E	02/19/2007	0.297	110.35	3 – 86 (11 settings)
3001226F	02/19/2007	0.297	131.08	3 – 86 (11 settings)
30012270	02/19/2007	0.297	171.32	3 – 86 (11 settings)
30012271	02/19/2007	0.297	201.35	3 – 86 (11 settings)

The raw PFM 5 data were retrieved from the SPIRE archive database at RAL for both the photometer and spectrometer arrays using the export tool of QLA (version 3.3). Tables 4-1 and 4-2 summarize, respectively, the photometer and spectrometer data analyzed in this chapter, where the data columns are, from left to right: OBSID, the date of the measurement, the average He^3 fridge temperature (T_subk) over the exposure time of the measurement derived from the housekeeping (HK) telemetry, the bias frequency (f_bias), and the range of the *peak* bias voltages (V_bias) with the number of individual bias voltages given in the bracket. For the photometer, the individual peak bias voltages for each detector array are around 0.0, 3.0, 7.0, 11.5, 15.5, 20.1, 25.6, 31.7, 40.3, 51.9, 64.5 and 86.2 mV. For the spectrometers, they are around 4.8, 14.5, 22.8, 31.1, 40.1, 51.2, 62.9, 80.2, 103.0, 128.7, and 171.5 mV. Not every measurement covers the entire set of these bias voltages. The actual number with valid data is given in the bracket in the last column of Table 4-1 or 4-2.

The PFM 5 data analyzed here cover a total of 103 and 96 points in the parameter space of (T_sub, f_bias, V_bias) for the photometer and spectrometer, respectively.

Table 4-2: List of Spectrometer Dark Noise Measurements.

OBSID	Date	T_subk (K)	f_bias (Hz)	V_bias (mV)
3001223C	02/17/2007	0.286	100.68	4.8–171.5 (11 settings)
3001223D	02/17/2007	0.286	161.42	4.8-128.6 (10 settings)
3001223E	02/17/2007	0.286	212.29	4.8-171.5 (11 settings)
3001223F	02/17/2007	0.286	275.09	4.8-171.5 (11 settings)
30012240	02/17/2007	0.286	305.17	4.8- 40.1 (5 settings)
30012242	02/17/2007	0.295	100.68	4.8-171.5 (11 settings)
30012243	02/17/2007	0.295	161.42	4.8-128.6 (10 settings)
30012244	02/17/2007	0.297	212.29	4.8-171.5 (11 settings)
30012245	02/17/2007	0.297	275.09	4.8-103.1 (9 settings)
300122C6	02/21/2007	0.297	100.67	4.8-171.5 (11 settings)
300122C7	02/21/2007	0.297	161.42	4.8-128.6 (10 settings)
300122C8	02/21/2007	0.297	212.29	4.8-171.5 (11 settings)
300122C9	02/21/2007	0.297	275.09	4.8-103.1 (9 settings)
300122CA	02/21/2007	0.297	305.17	4.8- 63.0 (7 settings)

4.2 Processing

For each OBSID, we obtained the nominal housekeeping data in converted form and the full array science data and associated offsets in raw format. The basic data processing was done using the IDL-based bolometer analysis package originally developed at IPAC (Schulz, Zhang et al. 2005). We first divided each observation into individual timelines according to the STEP signal in the HK parameter file.

Each resulting timeline corresponds to a constant bias voltage setting and spans about 500 seconds in time. The signals S_{raw} and offsets S_{offset} were then converted to Volts, using the following equations:

$$\text{Signal} = 5.0 * S_{raw} / [(2^{16} - 1) * 12 * \kappa], \text{ and} \quad (1)$$

$$\text{Offset} = 5.0 * [52428.8 * S_{offset} - 16384.0] / [(2^{16} - 1) * 12 * \kappa), \quad (2)$$

where $\kappa = 454.0$ for the photometer arrays and $\kappa = 294.0$ for the spectrometer arrays. We note that the correct values to be used in the pipeline are $\kappa = 456.6$ and 294.56 respectively. As the effect is negligible for this analysis we did not correct this anymore. We also note that we did not apply the correction for stray capacitances, which is not yet conclusively determined, but which is estimated to be below per-cent level for the lower bias frequencies. For higher bias frequencies the effect on the resulting thermistor temperatures can be significant however and will need further investigation.

The converted signal and offset voltages were then co-added. Each signal timeline was subsequently plotted on screen for visual inspection. In some cases, the first timeline and/or the last is apparently unusable, probably as a result of poor readout synchronization. These bad timelines were left out from Table 4-1 or 4-2 and from our further analysis. Each of the remaining "good" timelines was de-glitched and then further divided into segments corresponding to a lower limiting frequency of 0.01Hz. These segments were each Fourier transformed, normalized and then quadratically co-added to yield the final power spectrum. For each channel power spectrum, a plateau white noise, σ, was defined to be the median value between 0.5 and 2.0 Hz. The power spectrum at lower frequencies was fit into a sum of σ and a 1/f component. The frequency where the two components equal to each other is identified as the 1/f knee frequency, f_knee.[2]

[2] See caveats in chapter about 1/f noise and temperature instabilities.

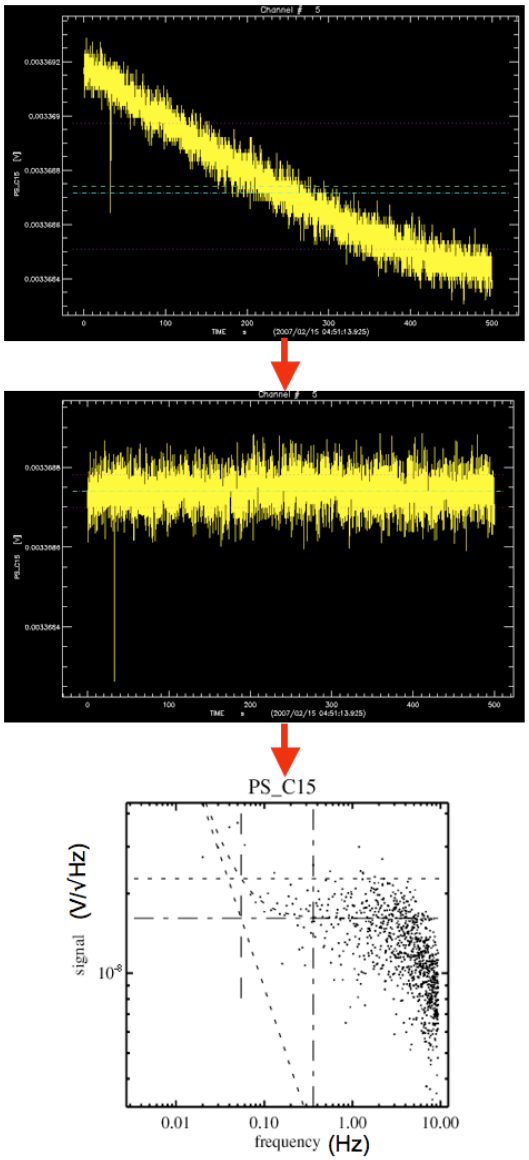

Figure 4-1 : A sketch of the noise analysis process on one photometer channel (PSW_C15): a signal timeline of about 500 sec long in the upper plot shows some temperature drift. The drift-removed timeline, which is displayed in the middle plot, was then split into segments of 100 sec each, followed by a Fourier transform on each segment. The individual segmental power spectra are co-added quadratically to produce the final power spectrum shown in the bottom plot, from which the plateau white noise (horizontal dash-dotted line) and 1/f knee frequency (left vertical dashed line) are determined. The upper two plots are screen shots from a visualization tool. The X-axis ticks are marked at 0, 100, 200, 300, 400, and 500 seconds. The Y-axis ticks are at 3.3684, 3.3686, 3.3688, 3.3690 and 3.3692 mV in the upper plot, and at 3.3684, 3.3686 and 3.3688 mV in the lower plot. The light blue and green dashed lines in the upper or middle plot represent the data median and mean.

4.3 JFET Noise

To optimize the operating point of the JFET pre-amplifiers, the pure amplifier noise was measured as the white noise plateau level with the bolometers at temperatures of ~4 K. At this temperature the resistance

of the bolometers is negligible compared to that of the load resistors, and thus the bolometer noise. The electronic signals under these circumstances were very stable and the noise measurement was straight forward. The JFET bias was varied in 11 steps for both photometer and spectrometer in the prime instrument configuration over the range of -2.4746 to -1.4693 V and: -2.5098 to -1.4902 V in the redundant configuration. Each JFET module comprises 24 channels. For each one an optimum bias can be selected. The correct choice of the JFET bias voltage is not critical, but should be part of the initial setup of the system to achieve the right working temperature for the JFETs. Otherwise spontaneous spiking and excess can appear, as observed in test campaigns prior to PFM 5. We note the determined optimum JFET biases (Vss) for each module in Table 4-3 the corresponding measured electronic noise levels in prime and redundant configuration in Tables 7-1 and 7-2. These values apply strictly only to the experimental setup at RAL and will need to be re-determined after integration into the spacecraft to account for the different resistances of the spacecraft cryo-harness.

Table 4-3: Optimum JFET bias settings determined for each of the photometer and spectrometer modules (24-channels) and the PTC channel. The actual settings that were commanded during the PFM 5 campaign are given as "setting 1" and "setting 2". The difference between these two settings and the channel numbers of the modules appear in the last two columns. Larger differences are highlighted in bold font.

	optimum	setting 1	setting 2	difference	channels
PSW-V1	-1.68	-1.68	-1.71	0.03	1..24
PSW-V2	-1.58	-1.59	-1.61	0.02	25..48
PSW-V3	-1.58	-1.37	-1.61	**0.24**	49..72
PSW-V4	-1.68	-1.59	-1.71	*0.12*	73..96
PSW-V5	-1.78	-1.78	-1.80	0.02	97..120
PSW-V6	-1.68	-1.59	-1.71	*0.12*	121..144
PMW-V1	-1.68	-1.68	-1.71	0.03	193..216
PMW-V2	-1.88	-1.59	-1.90	**0.31**	217..240
PMW-V3	-1.68	-1.59	-1.61	0.02	262..285
PMW-V4	-1.88	-1.88	-1.90	0.02	241..261
PLW-V1	-1.78	-1.59	-1.80	**0.21**	145..168
PLW-V2	-1.58	-1.37	-1.61	**0.24**	169..192
SSW-V1	-1.68	-2.07	-1.59	**-0.48**	1..24
SSW-V2	-2.05	-1.59	-2.07	**0.48**	25..48
SLW-V1	-1.58	-1.68	-1.68	0.00	49..72
PTC_V	-1.48	-1.49	-1.51	0.02	286..288

Unfortunately the optimum JFET biases were not correctly implemented for the first part of the PFM 5 campaign, and were only corrected starting from BBID 0x300122C6 for the spectrometer and even later for the photometer from BBID 0x0x30012447. The net effect was that for 6 modules out of 12 photometer modules the JFET biases were not correct for all photometer noise measurements that are analyzed here. For the lower temperature measurements of the spectrometer the two SSW modules had a non-optimal JFET bias. This likely affected the stability of at least some channels, in the modules highlighted in bold font in Table 4-3.

4.4 Temperature Drift Removal

The presence of the uncorrected temperature drift in the data leads to an overestimate of both the intrinsic 1/f knee frequency f_knee and the white noise level σ. We removed the thermal drift empirically as described in the previous chapter using the signals of both thermistor pixels (T1+T2 method) and a spline smoothing with a time interval of 5 sec before a noise analysis was done.

Since PMW_T2(219) is inactive, only PMW_T1(194) was used for the correction of PMW detector channels. Furthermore we note that for the photometer noise measurements, both thermistor channels were saturated at V_bias > 60 mV. As a result, some of the highest bias voltage settings given in the last column of Table 1 may not have their noise statistics presented in the remainder of this report.

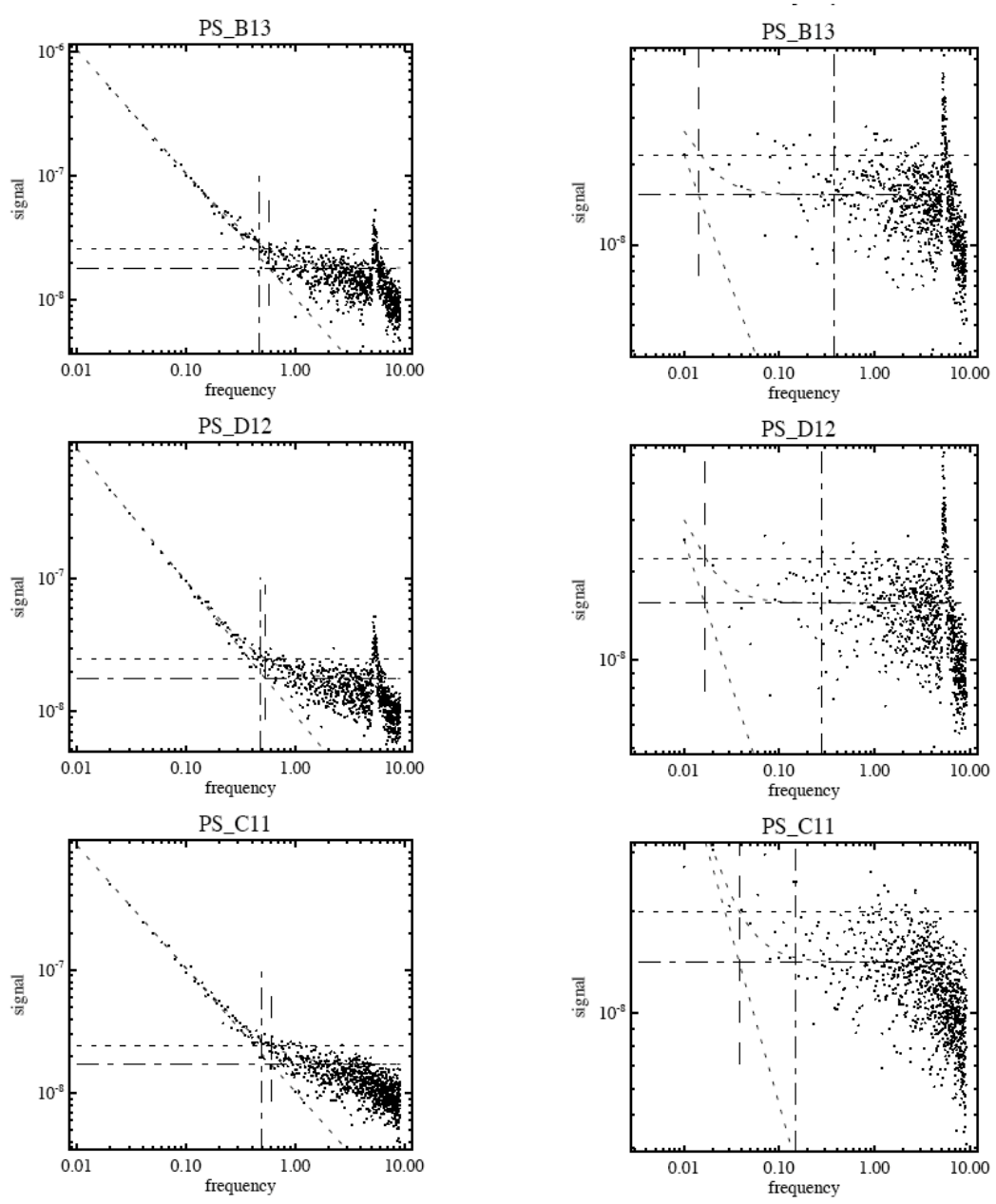

Figure 4-2 : Power spectra prior to temperature drift removal (left column) and after (right column) for a set of PSW channels. The abscissa is the frequency in Hz, and the ordinate is the noise power in V/√Hz. Note that the plots here have different Y-axis scales in the left and right columns.

Fig. 4-1 illustrates the data process on a PSW channel incorporating the temperature drift removal. The 1/f knee frequency f_knee and the plateau white noise are indicated in the figure by the vertically dashed

line and the horizontal dash-dotted line, respectively. The high frequency roll-off is due to the 5 Hz low-pass filter in the photometer electronics. Fig. 4-2 compares the power spectra for some representative PSW channels prior to and after the temperature-drift removal. In the remainder of this chapter, we use only the plateau white noises after removal of the low-frequency temperature drifts, unless noted.

Calculated thermister temperatures

Photometer (OBSID=30012150, T_{sub}=286mK, f_{bias}=80.37Hz)

-- Peak Bias Voltage (mV) --			Inferred baseplate temperatures (K)				
PSW	PMW	PLW	PS_T1	PS_T2	PM_T1	PL_T1	PL_T2
0.0000	0.0000	0.0000	...	...	...	...	...
3.0074	3.0265	3.0390	0.330	0.330	0.326	0.326	0.326
7.0172	7.0618	7.0911	0.330	0.330	0.326	0.326	0.326
11.5282	11.6015	11.6496	0.331	0.330	0.326	0.326	0.326
15.5380	15.6368	15.7017	0.331	0.330	0.326	0.326	0.326
20.0491	20.1765	20.2602	0.331	0.331	0.327	0.326	0.326
25.5626	25.7250	25.8318	0.332	0.331	0.327	0.327	0.327
31.5773	31.7780	31.9099	0.332	0.332	0.327	0.327	0.327
40.0982	40.3530	40.5205	0.333	0.332	0.327	0.327	0.327
51.6264	51.9544	52.1701	0.345	0.333	0.328	0.328	0.328
64.1571	64.5647	64.8328	0.366	0.350	0.329	0.329	0.329
85.7098	86.2545	86.6125	0.393	0.377	0.340	0.352	0.359

Spectrometer (OBSID=300123C, T_{sub}=286mK, f_{bias}=100.68Hz)

Peak Bias Voltage (mV)		Inferred baseplate temperatures (K)			
SSW	SLW	SS_T1	SS_T2	SL_T1	SL_T2
4.8419	4.8428	0.296	0.296	0.300	0.295
14.5258	14.5285	0.296	0.297	0.301	0.296
22.8263	22.8304	0.297	0.298	0.302	0.296
31.1268	31.1324	0.297	0.299	0.303	0.296
40.1189	40.1262	0.298	0.300	0.304	0.297
51.1862	51.1955	0.299	0.301	0.306	0.297
62.9452	62.9566	0.301	0.308	0.325	0.298
80.2379	80.2524	0.321	0.330	0.349	0.299
103.0642	103.0828	0.338	0.352	0.373	0.301
128.6573	128.6806	0.355	0.372	0.394	0.312
171.5431	171.5741	0.378	0.398	0.423	0.330

Figure 4-3 : Illustration of the calculated thermistor temperatures for some photometer measurements at the top and for some spectrometer data at the bottom.

4.5 Thermistor Temperatures and Detector Noise Equivalent Power

In order to compare bolometer noises in a way that is appropriate for astronomical applications, we need to derive for each bolometer channel, the noise equivalent power (NEP) in units of W/√Hz from the measured noise (σ) in V/√Hz. This is given in Eq. (3):

$$NEP = \sigma / S, \qquad (3)$$

where S is the detector responsivity in units of V/Watt. We resort to using Mather's dark bolometer model with the parameters R*, Δ, G_0, and β as determined at assembly level with BoDAC to derive the responsivity S, and the predicted noise. Noise and responsivity depend on (i) the temperature of the base plate of the bolometer array Tb (also called bath temperature), and (ii) the DC equivalent bias voltage

V_bias/√2. In addition the amplifier voltage noise Vn adds quadratically to the bolometer noise. We use Vn = 10 and 9 nV/√Hz for the photometer and spectrometer, respectively.

We approximate the thermal bath temperature Tb as the average temperature of the two thermistor channels. The temperature of a thermistor channel is calculated from the measured average bolometer voltage, and the bias voltage using the bolometer model. The resulting temperatures are usually very similar for the two thermistors T1 and T2. Fig. 4-3 shows some examples of the calculated thermistor temperatures for both photometer and spectrometer. At the lowest bias voltages, the inferred array temperatures are about 40 mK above T_subk for the photometer arrays, but only 10 mK above T_subk for the spectrometer arrays. These numbers are consistent with the finding presented in Nguyen et al. (2007) that there is a temperature drop of ~30 mK between the photometer bolometer assembly and the He^3 fridge.

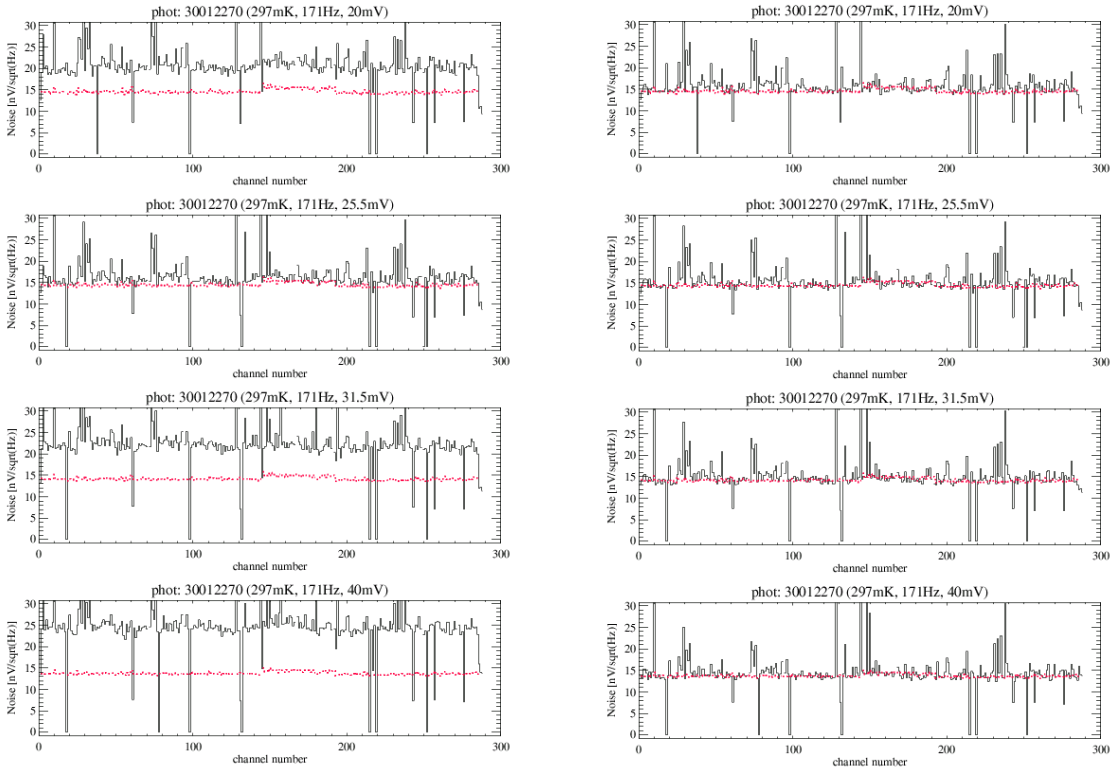

Figure 4-4 : Plots of detector channel noises as a function of QLA channel number for the photometer, where PSW runs channels from 1-144, PLW from 145-192 and PMW from 193-288. The data is from OBSID 30012270 taken at T_subk = 297 mK and f_bias = 171.33 Hz. Each plot is for a different bias voltage as labelled at the top of the plot. The solid histograms stand for the measured noises and the red dotted lines give the model predictions. As a comparison, we show the results prior to and after the removal of the temperature drifts on the left and right side, respectively. The channels with a measured noise lower than 10 nV/√Hz in these plots are those with an abnormal load curve (see Tables 2-1 and 2-2). Those inactive channels have a value of zero in these plots.

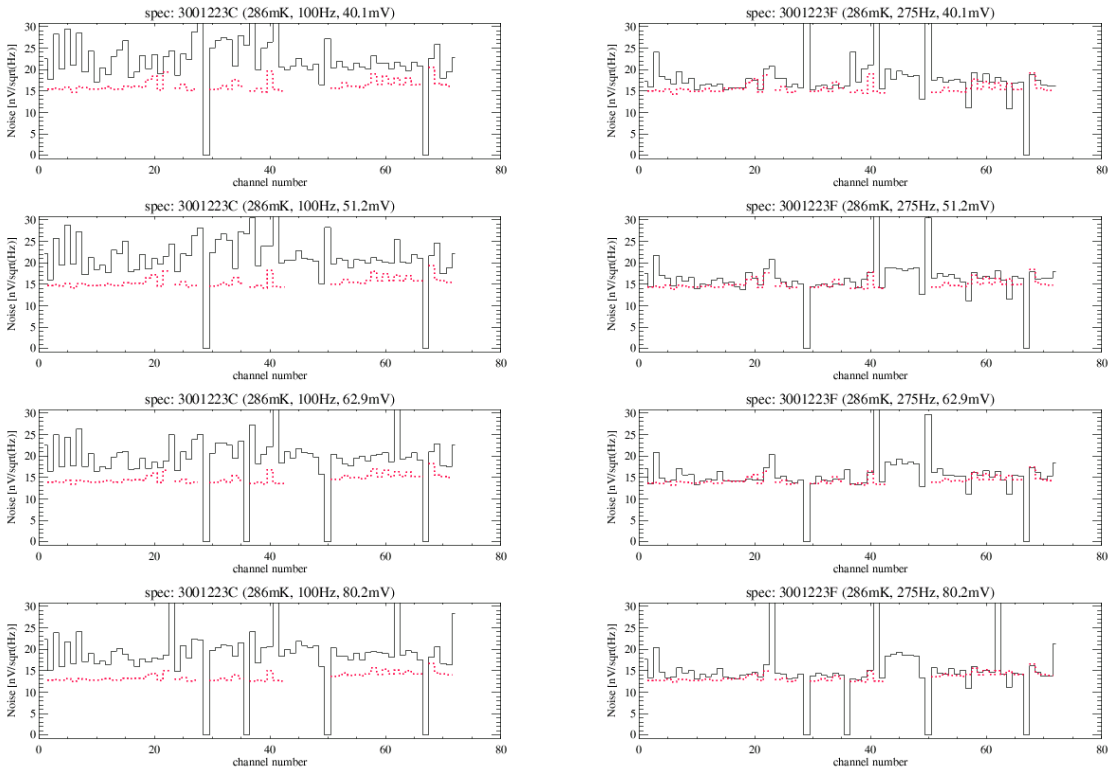

Figure 4-5 : Plots similar to left column of Fig. 4-4, but for the spectrometer after the temperature drifts have been removed. SSW spans channels from 1-42 and SLW from 49-72. The left panel displays the results from OBSID 3001223C (T_subk = 286 mK, f_bias = 110.68 Hz) while the plots in the right panel from OBSID 3001223F (T_subk = 286 mK, f_bias = 275.09 Hz). Model noise values are not available for some channels. Note that the model values agree less with the measurements in the plots on the left side (f_bias = 100.68 Hz) than in those on the right side (f_bias = 275.09 Hz) It is not clear whether this is the effect of variable noise contributors from the lab environment or whether this can be attributed to the missing correction for stray capacitances at the higher bias frequency.

The model predicted noises can be compared with the observed noises to see how well the model agrees with the measurements and how well the predicted astronomical sensitivities can be trusted. There is generally a quite good agreement (i.e., within ~10%) between the measured and predicted noises for the photometer, especially at V_bias > 10mV. Fig. 4-4 shows the model vs. measurement comparisons for all the photometer channels for f_bias = 171.33 Hz and a number of bias voltages. Results from both, prior to (left column) and after the temperature drift removal (right column) are to illustrate the significance of the temperature drift effect.

For the spectrometer, the agreement between the model and the measurements is not as good as for the photometer, especially at f_bias = 100.68 Hz. Fig. 4-5 displays some spectrometer examples of model vs. measurement comparisons for two bias frequencies, (a) f_bias = 100.68 Hz and (b) f_bias = 275.09 Hz. All the results in Fig. 4-5 are after the temperature drift removal. In the case of (a), the measured noises are clearly worse than the model predictions. In contrast, the overall agreement between the data and model is fairly good in (b). We noticed that another spectrometer measurement (OBSID = 300122C6) using the same bias frequency as that in (a), but on a different date, shows a much better agreement with the model prediction. It is therefore possible that additional noise sources or instability may have contributed to the data in (a).

4.6 Noise Statistics

It is evident from channel noise plots (e.g., Fig. 4-5) that, except for a few individual channels that are either abnormal or particularly noisy (see Tables 2-1, 2-2), the detector noises do not vary significantly over each bolometer array and across the arrays. The r.m.s. channel-to-channel variations are of the order of 10-15% for either the photometer or the spectrometer. While we give typical noise values for each detector channel at the end of this report, we analyze in this section the median noise across all the channels for a given bolometer array. It is also advantageous to express the noises in terms of NEP, via eq. (3), with the caveat that at the low end of the tested bias voltage range and for some spectrometer measurements, the model-predicted noises do not fully account for the measured noises.

Figs. 4-6 to 4-8 show the measured median array NEP on the left and the ratio of this to the median model-predicted NEP on the right, each as a function of the peak bias voltage, for all the measurements of the photometer arrays PSW, PMW and PLW, respectively. Different symbols are used to distinguish different bias frequencies, while the black and red symbol colors indicate T_subk of 286 and 297 mK, respectively. Note that the measurements at V_bias > 60 mV are not shown here as they contain saturated thermistor channels. Clearly, the left-hand-side plots in these figures show a well-defined minimum NEP for each array at each T_subk. These minima are located at V_bias = 20 to 25 mV for all three photometer arrays.

The lower T_subk led to lower noises as expected. The minimum overall NEPs reached at the optimal V_bias for T_subk = 286 mK are on the order of 4.6, 4.6, and 4.3 x 10^{-17} W/√Hz for PSW, PMW and PLW, respectively.

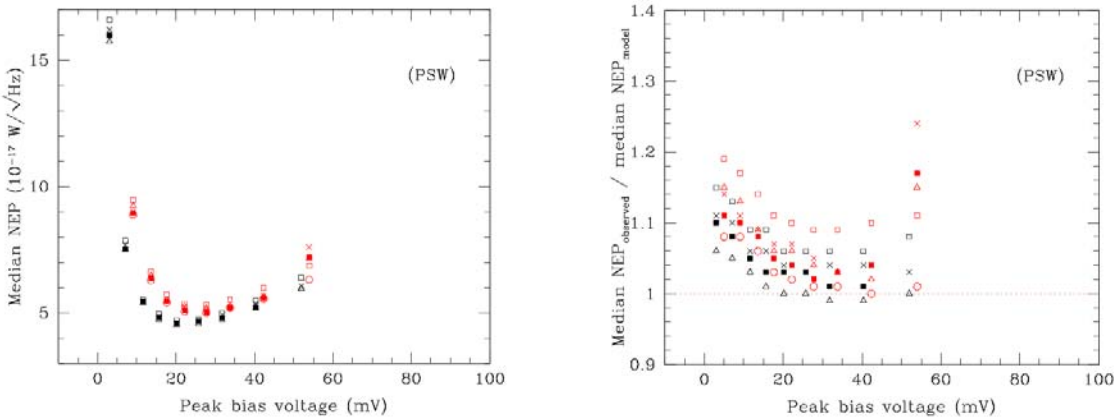

Figure 4-6 : Plots of the observed median array NEP on the left and of the ratio of the observed median array NEP to the model-predicted median array NEP on the right, as a function of the peak bias voltage applied to PSW. The different symbols stand for different bias frequencies: 80.4Hz (open squares), 110.4Hz (crosses), 131.1Hz (filled squares), 171.3Hz (triangles) or 201.4Hz (circles). The black and red symbols represent T_subk = 286 and 297mK, respectively. For the purpose of clarity, there is a slight horizontal offset between the black and red symbols.

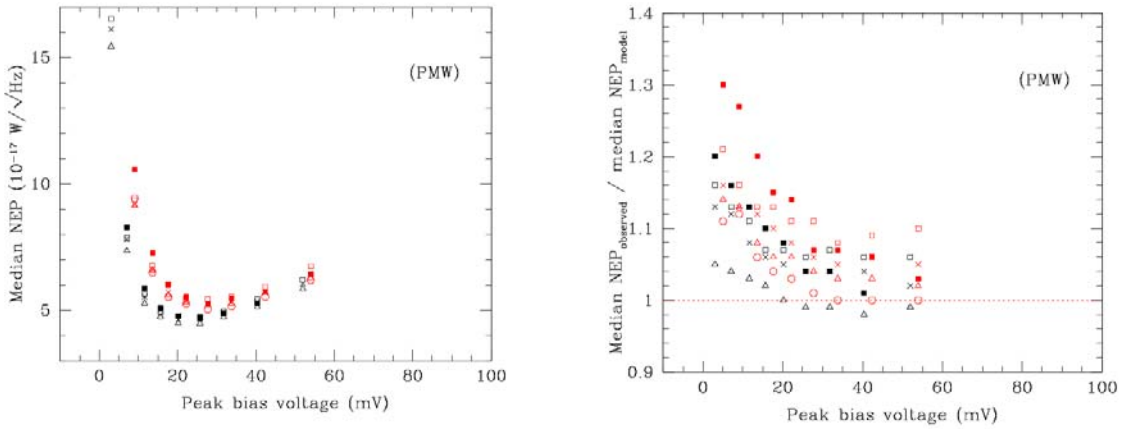

Figure 4-7 : Similar to Fig. 4-6, but for PMW.

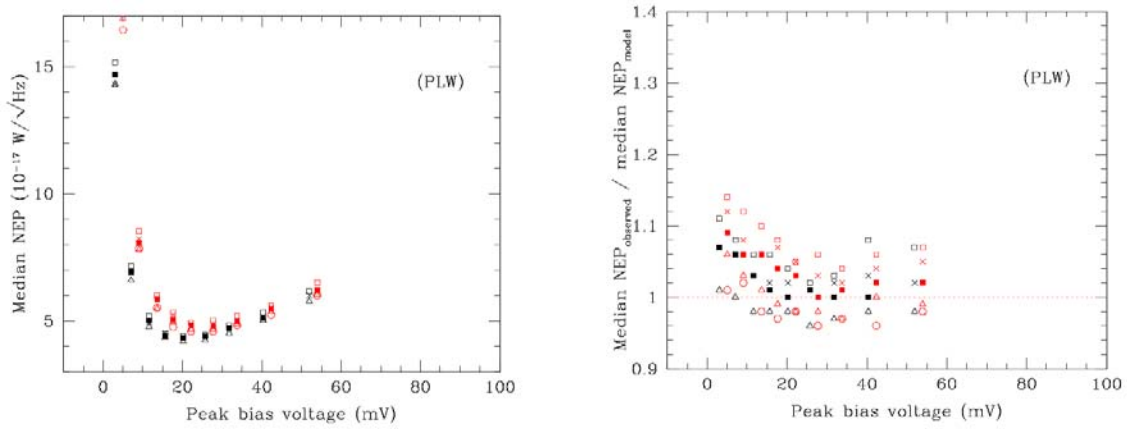

Figure 4-8 : Similar to Fig. 4-6, but for PLW.

The right-hand-side plots in Figs. 4-6 through 4-8 show that the agreement between bolometer models and the measurements is generally better than 10%, except for some cases with V_bias < 10 mV. The measured detector noises also show a small dependence on f_bias. This becomes clearer in the right-hand-side plots in Figs. 4-6 to 4-8 as the bolometer model we used is independent of f_bias: the higher the bias frequency f_bias, the lower the measured noises are observed. At V_bias ~ 20 mV this frequency dependency leads to a noise difference of about 3-4% over the f_bias range tested here. It is not clear at this point whether this is a manifestation of the yet uncorrected signal dependence on frequency due to stray capacitances.

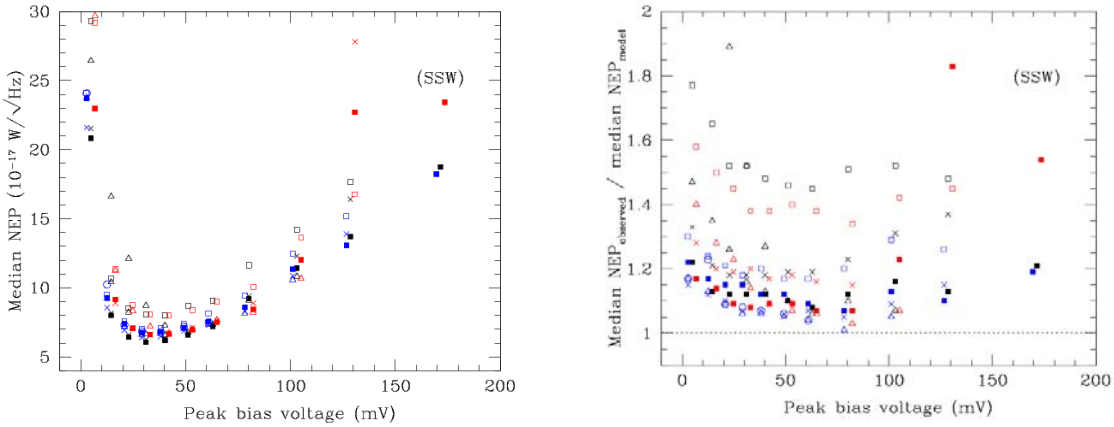

Figure 4-9 : Similar to Fig. 4-6, but for the spectrometer array SSW. The different symbols stand for different bias frequencies: 100.68Hz (open squares), 161.42Hz (crosses), 212.29Hz (filled squares), 275.09Hz (triangles) or 305.17Hz (circles). The black, red and blue symbols represent the noise measurements at T_subk = 286 and 297mK, and the dark load curve measurements at T=297mK, respectively. For clarity, small horizontal offsets are added in this plot to visually separate the three color-coded data sets.

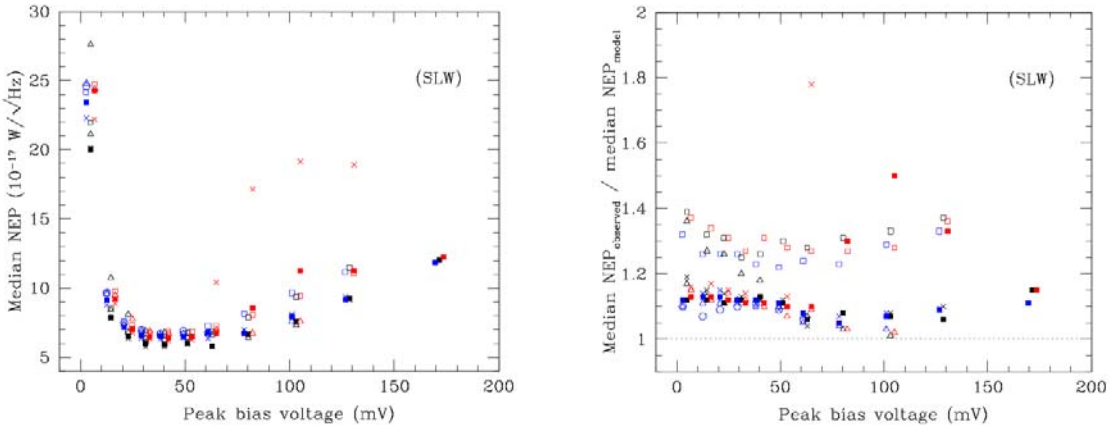

Figure 4-10 : Similar to Fig. 4-9, but for the spectrometer array SLW.

Figs. 4-9 and 4-10 show plots similar to Figs 4-6 through 4-8, but for the two spectrometer arrays. There appears to be some dependence of the measured noise on the bias frequency in the case of SSW. But the frequency dependency is much less in the case of the dark-load curve measurements (i.e., the blue data points in Fig. 4-10) than in the other two data sets (black and red). So it is possible that some extra noise terms may be present in some of the measurements shown in black or red in Figs. 4-9 and 4-10. In spite of this uncertainty, the data points in the left-hand-side plot of Fig. 4-9 or 4-10 still form a well-defined frontier consisting of all the minimum NEPs at the bias voltages used. The minimum of this frontier occurs at V_bias ~ 35 mV for both SSW and SLW. At this optimal bias voltage, the minimum overall NEPs are on the order of 6 x 10^{-17} W/√Hz for both SSW and SLW.

The right-hand-side plots in Figs. 4-9 and 4-10 show that the agreement between bolometer models and the measurements could be as good as 5% in some measurements, however, the scatter is fairly large here. Around the optimal bias voltage of 30 to 35 mV, most of the measurements appear to agree with the model predictions to about 10-15%. This large scatter also makes it difficult to assess quantitatively how the noises depend on f_bias, which is expected to be only marginal.

To give typical channel noises under the optimal bias setting, Table 7-1 in Annex A gives the measured photometer channel noises in nV/√Hz and NEP's in nW/√Hz for the case of (T_subk, f_bias, V_bias) = (0.286K, 80.37Hz, 20.18mV) from the observation of OBSID=30012150. Similarly Table 7-2 lists the same parameters for the spectrometer channels for the case of (T_subk, f_bias, V_bias) = (0.286K, 212.29Hz, 40.12mV) from the measurement of OBSID=3001223E. The columns in each table are, from left to right, bolometer channel number, JPL channel name, measured noise, model-predicted noise, NEP from the measured noise. We do not show 1/f noise values that turned out to be too noisy and unreliable from this dataset and refer to Chapter 3 in that respect. These tables should provide some quantitative guidance on whether a particular channel is good, slightly noisy or very noisy. Note that those inactive or abnormal channels do not have a valid entry under the measured noise, and that not all channels have a valid model-predicted noise.

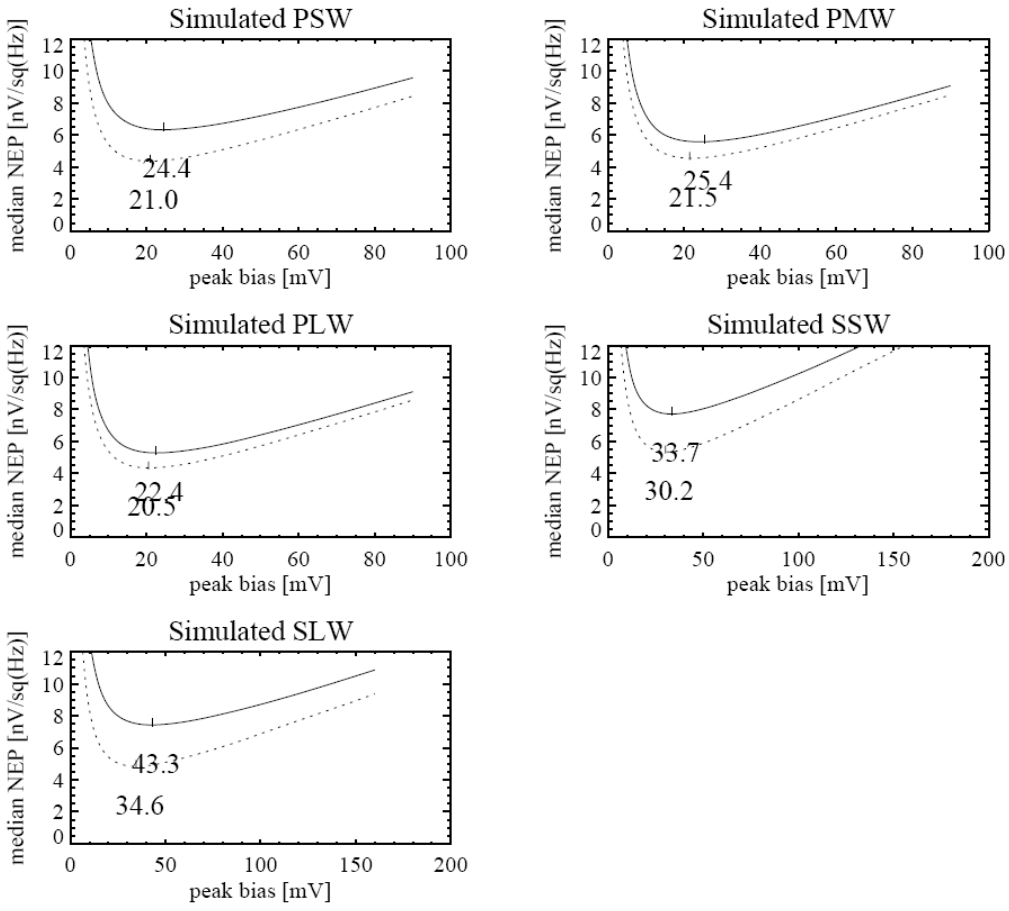

Figure 4-11: Optimum bias voltages found with Mather's model calculating the array median of all NEP's depending on bias voltage for dark conditions and under optically loaded conditions. The solid curves are optically loaded; the dotted curves are for dark conditions.

4.7 Optimum In-Flight Bias

The noise parameters established from PFM 5 measurements apply strictly only to dark conditions. Due to the "warm" 79-90 K telescope mirror, the detectors will experience a substantial optical load during the mission. The good agreement of the model predictions with the measured noise data under dark conditions has shown its general applicability and reliability. We use it in the following to predict the in-flight optimum bias values. Since the expected telescope emissivity is considerably lower than at the time the instrument was designed, we used the new in-band optical loads 1.7, 1.0, 1.2, 4.1, and 4.9 pW for PSW, PMW, PLW, SSW, and SLW respectively. We used bath temperatures of 330 mK for the photometers and 296 mK for the spectrometers, which are temperatures that were typical for the non-heated tests during PFM 5 (see Figure 4-3).

4.8 Summary and Conclusions for White Noise

We have analyzed the dark measurements in the PFM 5 test campaign. The data cover all the SPIRE PFM bolometer arrays, two He^3 fridge temperatures (T_subk = 286 and 297 mK), a set of bias frequencies (f_bias = 80-201 Hz for the photometer and 100-205 Hz for the spectrometer) and bias voltages V_bias = 0-86.6 mV for the photometer and 4.8-171.5 mV for the spectrometer). We derived appropriate bolometer channel noises under each set of control parameters (T_subk, f_bias, V_bias) , compared them with the bolometer model predictions, and identified the array optimal bias settings that lead to the least overall detector noises observed. We summarize our results as follows:

1. A temperature-based signal drift is seen in many of the PFM 5 dark noise measurements, and this drift affects significantly the 1/f knee frequency and plateau white noise determinations. This temperature drift was empirically removed from the signal of each bolometer channel based on the fact that it is largely linearly correlated with that of the thermistor channels. After this correction, the power spectra of the noise measurements are usually dominated by a flat white noise at frequencies greater than 0.05 Hz and below 2 Hz. For each bolometer channel, this flat white noise was taken as the detector noise.

2. Except for the special channels described in chapter 2 above, the measured detector noises are fairly uniform over each array and across the arrays. The r.m.s. variations are on the order of 10-15% for either the photometer or the spectrometer.

3. For the photometer arrays, the measured detector noises generally agree with those predicted from the EIDP bolometer models over the tested parameter space of (f_bias, V_bias, and T_subk) to within about 10%; for the spectrometer, the degree of agreement varies from 5% up, depending on individual measurements as some of them may be impacted by additional unknown noise terms.

4. As expected, the overall detector noises depend sensitively on V_bias. The optimal peak bias voltages in the dark appear to be 20-25 mV for the photometer arrays and ~35 mV for the spectrometer arrays. The measured noises also appear to increase slightly as f_bias increases. For the photometer arrays this frequency dependency accounts for a systematic noise difference of only 3-4% over the range of f_bias = 80-201 Hz. At the optimal bias voltages, the overall NEPs achieved are on the order of ~4.5x and 6x10^{-17}W/√Hz for the photometer and spectrometer arrays, respectively. These NEPs are within ~5 and 10% of the respective model predictions.

5. Under optically loaded conditions in-flight, we predict optimum bias voltages that are slightly higher than in the dark by 2-10 mV. The NEPs should increase by 20-50% depending on the detector array.

5. Microphonics

High S/N co-added power spectra of several hours display a number of features (presumably of microphonic origin) that sometimes vary from one night to the other. On first sight the overall picture of these features looks rather inconclusive, as they vary from one measurement series to the next, and may be driven by external influences of the test site at RAL. For investigation of microphonic resonances, it is more fruitful to analyze the dedicated tests with an applied mechanical excitation.

5.1 Data

For the spectrometer the OBSIDs 0x300122DD - 0x300122E6 were analysed. The dataset includes measurements with 10 bias frequencies between 75 to 305 Hz, at 4 bias amplitudes. The cryostat was excited mechanically with an electric thumper. The lab log notes: "microphonics excitation started with random noise filtered to 10Hz to 1 KHz".

For the photometer the OBSIDs 0x30012447 – 0x30012460 were analyzed. The dataset includes measurements with 26 bias frequencies between 75 to 201 Hz, at 3 bias amplitudes. The cryostat was excited mechanically: "Shaker input is white noise, band limited from 10 to 1000 Hz".

5.2 Analysis

The SPIRE signal chain has a wide bandwidth amplifier (20-4000 Hz for the spectrometer, 20-2000 Hz for the photometer), followed by a square-wave demodulator, and followed by a low-pass filter (25 Hz for the spectrometer, 5 Hz for the photometer). The demodulated and filtered "IF" band therefore has sensitivity to audio band noise around the demodulation frequency (= bias frequency) and its first few odd harmonics. Specifically, IF frequencies map to audio band frequencies as follows: $f = N \times f_{bias} \pm f_{IF}$, N = odd integer. The system has declining response to the higher harmonics as 1/N, not counting the pre-demodulation filter.

The data analysis procedure is as follows:

1. Generate noise spectra in V $Hz^{-1/2}$ for each frequency and amplitude, using thermistor-based temperature drift correction to partially cancel 1/f noise.
2. Plot IF noise spectra in the audio band, assuming a harmonic (N) and sideband (+ or – sign).
3. Search for spectral features which repeat in the audio band as the bias frequency changes.

5.3 Spectrometer Results

The figures below show typical noise spectra assuming that the noise comes from the lower sideband of the first harmonic of the bias frequency, or alternatively the upper sideband of the first harmonic.

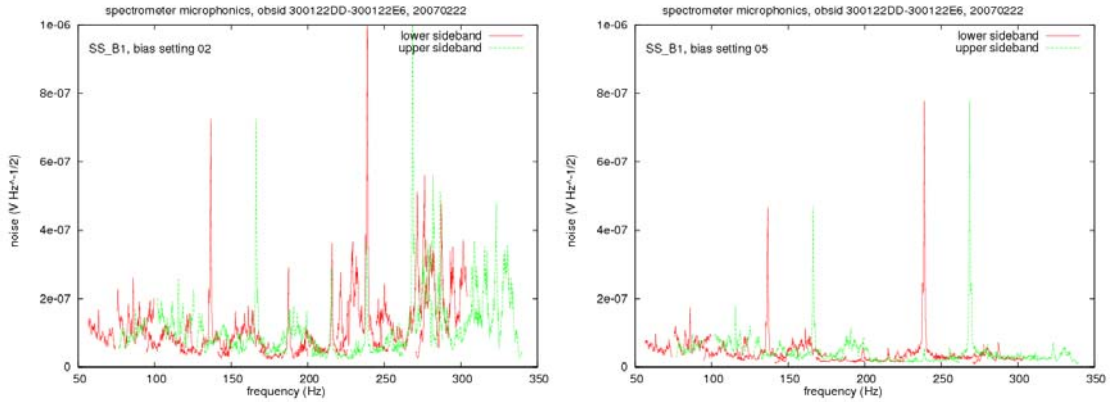

Figure 5-1: First harmonic noise spectra of short-wavelength spectrometer channel B1 for the lowest (left) and highest (right) bias amplitudes. Each curve is composed of 10 segments corresponding to the 10 bias frequencies. The locations of the strong features remain the same, but decrease in amplitude as the bolometer resistance decreases.

The signature in Figure 5-1 of a microphonic feature which is truly near the first harmonic of the bias frequency would be overlapping upper and lower sideband spikes, plus two false "image" spikes on each side of it. This signature is mostly absent, suggesting that many of the strong features are in higher harmonics.

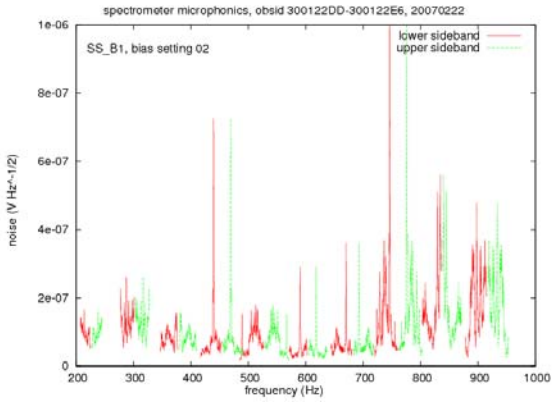

Figure 5-2: Noise spectra of SSW-B1 assuming that the noise comes from the third harmonic of the bias frequency. There is essentially no overlap between the sidebands at the 25 Hz bias frequency interval, so it is not possible to confirm third-harmonic features.

Since there is incomplete information for reconstructing the audio band spectrum from the IF spectra at the multiple bias frequencies, we use a cruder technique to highlight repeating microphonic features by simply multiplying the lower sideband spectra by the upper sideband spectra. The largest spikes will then correspond to features that repeat. Only in the first harmonic do the sidebands significantly overlap for the ~25 Hz interval of the bias frequency in these measurements, so we only multiply the first harmonic sidebands.

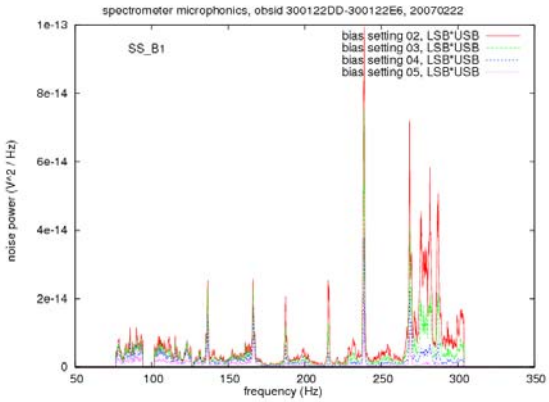

Figure 5-3: Product of first-harmonic upper and lower sideband spectra, as a function of bias amplitude, for SSW-B1. The ~235 Hz feature appears as the strongest "repeating" feature, although examination of Figure 5-1 shows that it repeats in frequency better than in amplitude, which casts some doubt on its origin in the first harmonic.

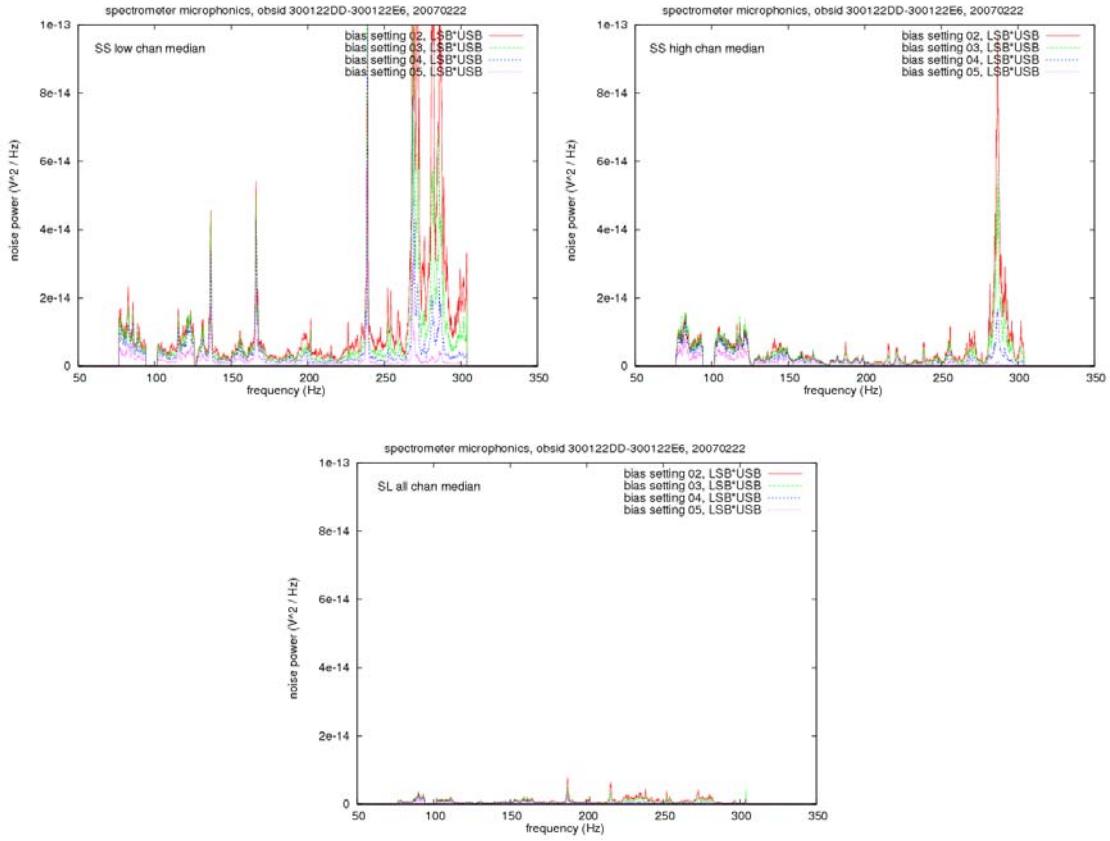

Figure 5-4: Median over ~24 channels (SSW low #, SSW high #, SLW) of the product of the first harmonic lower and upper sideband noise spectra.

The worst microphonic response is observed for bias frequencies between 230 and 300 Hz. The region near 200 Hz appears to have the least response. These are rough guidelines only; since it appears that much of the microphonic noise enters through harmonics ≥ 3 of the bias frequency, and the bias frequency settings used in these measurements only partially sample the audio band there, Figure 5-4

does not have strong predictive value for noise spectra at "in between" bias frequencies. Three times as many bias frequency settings would be needed to fully characterize the third harmonic audio band, five times as many for the fifth harmonic, etc.

5.4 Photometer Results

The figure below shows a typical noise spectrum assuming that the noise comes from the lower sideband of the first harmonic of the bias frequency, or alternatively the upper sideband of the first harmonic. In comparison with the spectrometer results, 1/f noise is stronger in the individual sideband spectra, despite the subtraction of the thermistor-correlated signal.

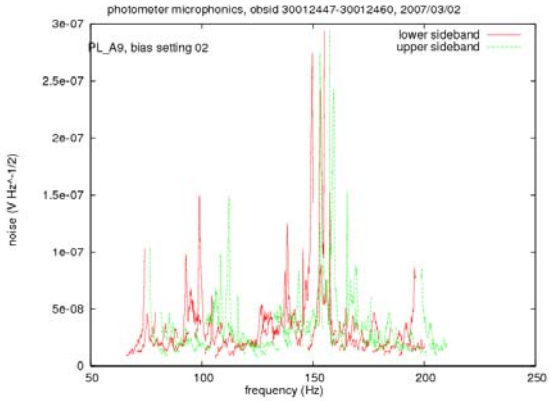

Figure 5-5. First harmonic noise spectra of long-wavelength photometer channel A9 for the lowest bias amplitude. Each curve is composed of 26 segments corresponding to the 26 bias frequencies. The microphonic feature at ~155 Hz repeats between the two sidebands, which supports the assumption that it is a first-harmonic feature. However, many other features do not repeat, suggesting that they are found near higher harmonics of the bias frequency.

Like the spectrometer data, there is insufficient bias frequency coverage to examine the repeatability of features near the third and higher harmonics of the bias. Once again, we use a simple technique to highlight features which repeat between the upper and lower sidebands: multiplying those two spectra.

5.5 Conclusions on Microphonics

The main conclusions are as follows:

1. At a single bias frequency, the microphonic response is repeatable and decreases with decreasing resistance.
2. Individual microphonic features often do not repeat as the bias frequency is changed, under the assumption that the features are located near the first harmonic of the bias frequency. This indicates that many of the features are located near higher, odd harmonics.
3. Channels 1-24 in the short-wavelength spectrometer have the greatest microphonic response, followed by channels 25-42 in the short-wavelength spectrometer. The microphonic response of the long-wavelength spectrometer is an order of magnitude lower.
4. For the spectrometer the worst microphonic response is observed for bias frequencies between 230 and 300 Hz. The region near 200 Hz appears to have the least response.

5. For the photometer the worst microphonic response is observed for bias frequencies between 130 and 180 Hz. The region near 125 Hz appears to have the least response.

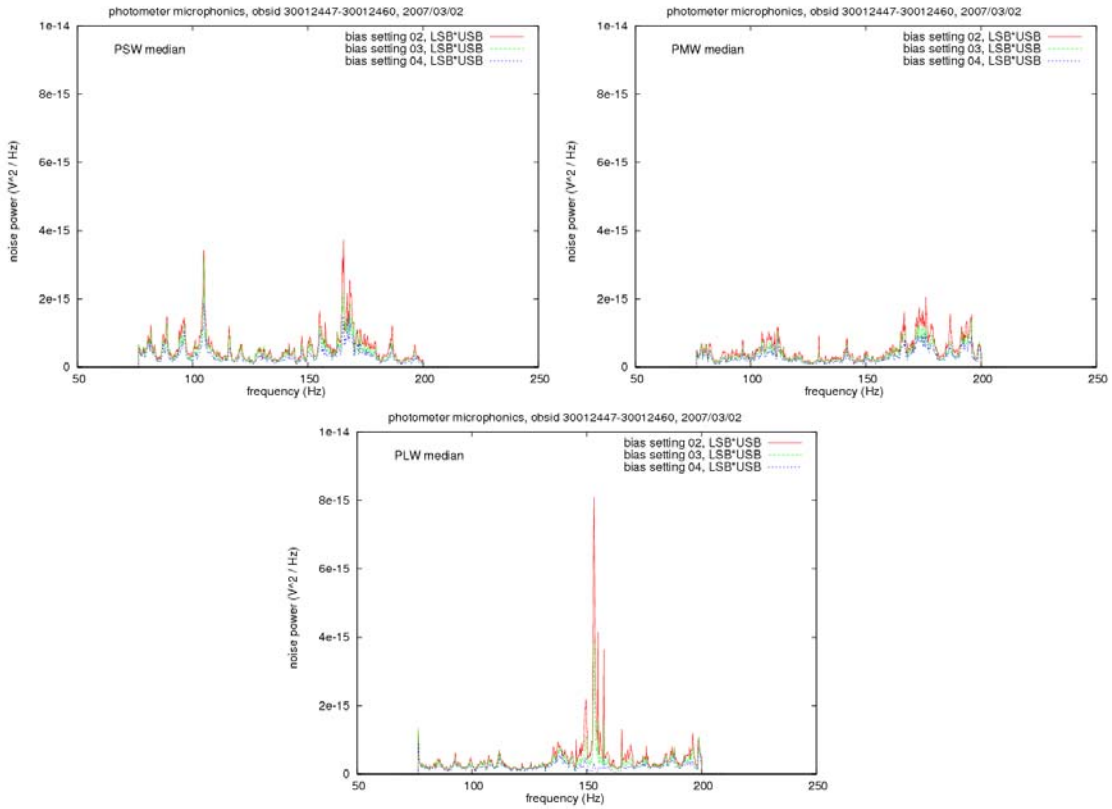

Figure 5-6. Median over the short-, medium-, and long-wavelength arrays of the product of the first harmonic lower and upper sideband noise spectra. Note the change in scale on the vertical axis compared to Figure 5-4; the photometer microphonics level is similar to the SLW microphonics level.

6. Comparison to Requirements

The results presented in this document can be compared to a few requirements for the SPIRE PFM detectors.

BDA-PER-01 *Maximum number of bad detectors in each BDA*:

The minimum performance requires <= 35, 22, 11, 9, and 5 bad detectors for PSW, PMW, PLW, SSW, and SLW respectively. The goal is 14, 9, 4, 4, and 2 respectively. We find 5, 1, 0, 2, 2 if we regard only non-recoverable pixels, which I well within the goals. Even including losses due to the test cryo-harness, which will be different after integration into the spacecraft, results in 8, 7, 0, 2, 3 lost channels, which is still within the goals except for the SLW.

BDA-PER-02 *The ratio of photon NEP due to radiation absorbed by the detector and total NEP, given as* $(NEP_{photon}/NEP_{tot})^2$:

This requirement is somewhat difficult to verify, as detector performance measurements on the ground were done either with too high background levels, or in the dark. As the comparison with the requirements is very dependent on assumptions about the telescope background in space and how excess noise scales with the model, we are limiting ourselves to a comparison of the dark noise data with the model predictions.

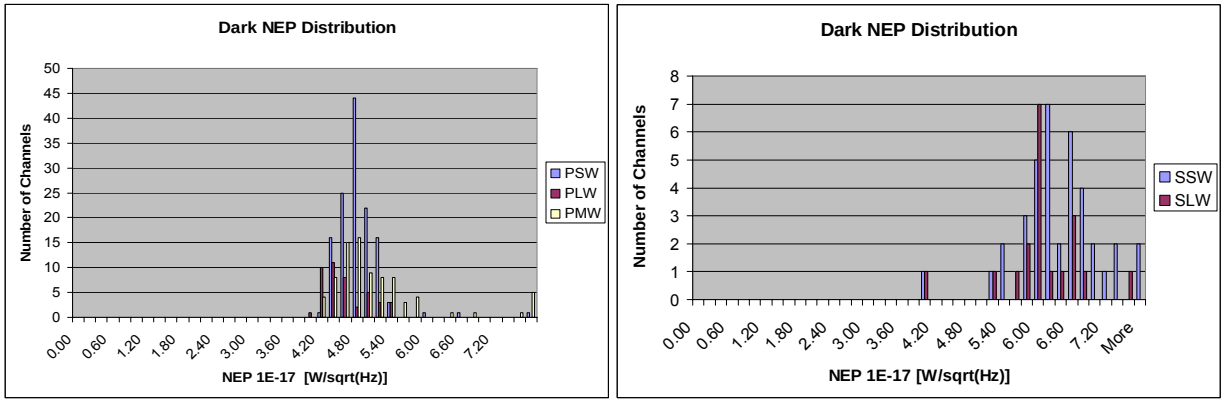

Figure 6-1: Distribution of Dark NEP values for photometer bolometers (left) and spectrometer bolometers (right).

Figure 6-1 shows the distributions of the measured NEPs for photometer and spectrometer pixels. The spectrometer distributions peak about a third higher than those of the photometer. However, the ratios of measured dark noise and expected noise according to the model are far more consistent with distributions of both, photometer and spectrometer peaking between 5% and 10% above the model predictions, which characterize the high quality of our model interpretation.

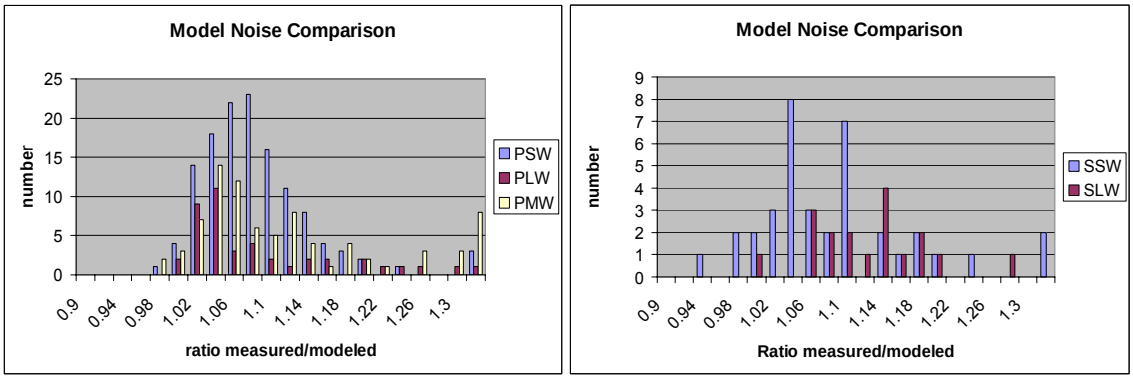

Figure 6-2: Distribution of ratios of measured and modelled dark noise values for photometer (left) and spectrometer (right).

BDA-PER-10 *The 1/f knee frequency:*

1/f knee frequencies are required to be below 0.1 Hz, with a goal of 0.3 Hz. The requirement was generally met, however with difficulty in the thermally relatively unstable laboratory environment. After

temperature correction the low frequency component is not any more of the 1/f form. However we can still define a 'knee', where the low frequency spectral component is equal to the white noise plateau. This is considerably lowered below the 50 mHz level for most channels; however, it will require more investigation to determine the exact "knee" frequencies and more generally the shape of the power spectrum below this frequency.

JFET-PER-01 *Median noise of JFET module over 100 – 300 Hz (nV/√Hz):*

The minimum performance value is 15 nV/√Hz and the goal is 7 nV/√Hz. All channels meet the minimum performance, and almost all stop short of the goal. The median noise values are 8.8394, 8.5856, 8.6872, 7.6414, 7.8443 nV/√Hz for the prime and 8.8594, 8.5710, 8.7371, 7.6793, 7.8242 nV/√Hz for the redundant configuration for PSW, PMW, PLW, SSW, and SLW respectively.

JFET-PER-02 *Maximum number of bad JFET pairs corresponding to each BDA:*

We did not find a detector channel that showed problems that could be traced back to intrinsic bad performance of a JFET pair. Increased noise and spontaneous spiking were observed in former test campaigns in some cases, due to incorrect Vss settings. These symptoms disappear with proper bias settings.

References:

Nguyen, H., Bock, J., & Schulz, B. 2007: PFM 5 -- Notes on Load Curve Analysis and Delta T Measured
Across Thermal Strip.

Schulz, B. 2006: SPIRE Science Verification Review: SPIRE Bolometer Array Noise Performance during PFM 1, 2 and 3 Test Campaign, Draft 3a

Griffin, M. 2006: SPIRE Science Verification Review: Bolometer Array Performance Estimation from EIDP Spreadsheets, Issue 1.0

Schulz, B., Zhang, L., Ganga, K., Nguyen, H., & Holmes, W., 2005: An Analysis Package for Bolometer Ground Testing, in ASP Conference Series V347, ed. by P. L. Shopbell, M. C. Britton, and R. Ebert (Pasadena, CA), p158.

Detector Subsystem Specification Document (SSSD - SPIRE-PRJ-000456, Issue 3.2, Jan. 7 2003) incl. modification by RFW HR-SP-JPL-RFW-002

7. Annex A

Table 7-1: Photometer channel noises from a noise measurement with (T_subk, f_bias, V_bias) = (0.286K, 80.37Hz, 20.1mV), which is near the optimal bias setting for the photometer arrays, of OBSID = 30012150. Permanently disabled channels are greyed out, and channels with any history of peculiarities during the test campaigns are marked in bold-face. The modelled noise as well as the NEP based on the modelled responsivity are given. Further we list the amplifier noise measured with warm (4 K) bolometers in prime and redundant instrument configurations for the optimum bias settings.

No.	Channel	Observed Noise (nV/sq(Hz))	Model Noise (nV/sq(Hz))	Observed NEP (1E-17) W/sq(Hz)	Warm Noise PFM 5	
					prime (nV/sq(Hz))	redundant (nV/sq(Hz))
1	PSW_R1	14.4	…	…	0.0000	0.0000
2	PSW_D16	15.5	15.15	4.40	8.5194	8.6477
3	PSW_T1	16.4	…	…	8.9681	9.0729
4	**PSW_B16**	22.3	14.98	6.50	11.4398	11.2853
5	PSW_C15	17.9	15.05	5.20	9.8288	10.0750
6	PSW_A15	15.1	15.09	4.38	8.6166	9.2751
7	PSW_D15	16.5	14.60	5.14	10.1493	10.4569
8	PSW_B15	16.0	15.04	4.66	8.5257	8.5696
9	PSW_C14	16.4	15.02	4.83	9.7556	9.3824
10	**PSW_D14**	16.4	16.27	4.22	9.8403	9.1771
11	**PSW_A14**	16.3	15.04	4.75	8.6076	8.4563
12	**PSW_A13**	14.7	14.98	4.23	9.0532	8.9950
13	PSW_B14	15.8	14.95	4.66	8.7589	9.1421
14	PSW_C13	14.9	14.92	4.47	8.3638	8.5377
15	PSW_B13	15.9	15.05	4.62	8.8561	8.5776
16	PSW_D13	15.8	15.08	4.77	9.1372	8.6999
17	**PSW_A12**	15.2	15.12	4.34	8.7837	8.5675
18	**PSW_C12**	…	…	…	0.0000	0.0000
19	**PSW_D12**	15.6	14.50	4.90	9.5163	10.0337
20	**PSW_B12**	16.1	15.07	4.82	16.4535	17.0041
21	PSW_E11	15.4	14.93	4.56	8.8332	8.7280
22	**PSW_A11**	15.1	14.92	4.36	8.7232	8.8205
23	**PSW_C11**	16.0	14.80	4.79	8.9558	10.1334
24	PSW_B11	15.8	14.48	4.99	9.5315	9.3036
25	PSW_E1	18.3	16.03	4.72	9.0224	9.5460
26	PSW_F1	15.8	15.06	4.59	8.7194	8.8371
27	PSW_T2	17.0	…	…	8.4077	8.3665
28	PSW_H1	15.4	14.97	4.52	8.3435	8.8689
29	PSW_G1	16.1	15.46	4.42	8.5050	8.5567

30	PSW_J1	16.0	15.05	4.66	8.6002	8.6269
31	PSW_H2	17.2	15.49	4.78	9.9100	9.5174
32	PSW_F2	15.9	14.68	4.87	8.8345	8.7127
33	PSW_J2	16.2	15.06	4.71	8.7459	8.8615
34	PSW_G2	15.9	15.04	4.70	8.7985	9.0149
35	PSW_H3	15.0	14.55	4.80	8.8661	8.5906
36	PSW_J3	17.2	14.98	5.04	9.1636	9.1498
37	PSW_E2	16.1	14.97	4.76	9.1238	9.2003
38	PSW_F3	16.8	15.26	4.83	9.5390	9.6216
39	PSW_G3	17.2	14.67	5.30	9.8398	10.0439
40	PSW_H4	16.2	15.12	4.78	8.5147	8.6556
41	PSW_J4	17.2	15.17	4.95	10.1300	10.0318
42	PSW_E3	16.5	15.19	4.67	9.5877	9.5111
43	PSW_F4	16.1	15.52	4.35	9.0026	8.8077
44	PSW_G4	16.8	15.30	4.80	8.5933	8.7455
45	PSW_H5	16.0	15.09	4.70	9.0225	8.8495
46	PSW_E4	15.8	15.14	4.62	8.8914	9.1790
47	PSW_J5	15.8	15.11	4.59	8.3382	8.2541
48	PSW_F5	15.4	15.26	4.32	8.7934	8.6734
49	PSW_D6	15.7	15.09	4.62	8.2938	8.2629
50	PSW_B6	14.7	14.62	4.50	8.3581	8.2334
51	PSW_C5	15.0	14.65	4.59	8.9064	8.6634
52	PSW_A5	15.8	15.03	4.59	8.5981	9.0691
53	PSW_E5	15.8	15.17	4.49	8.8604	9.2019
54	**PSW_B5**	17.0	15.94	4.30	9.2146	9.0978
55	PSW_D5	15.7	15.03	4.57	8.6948	8.7959
56	PSW_C4	15.1	14.48	4.79	9.1345	8.9329
57	PSW_A4	16.8	15.43	4.72	9.1339	8.9162
58	PSW_D4	16.4	14.60	5.01	9.3500	8.7564
59	PSW_B4	15.1	15.07	4.43	8.8952	8.4163
60	PSW_C3	16.3	16.28	4.18	9.4365	8.8623
61	**PSW_B3**	…	15.01	…	6.7688	6.7397
62	PSW_A3	15.3	14.94	4.56	9.3376	8.8277
63	PSW_A2	15.1	14.89	4.42	8.6849	8.5712
64	PSW_D3	15.4	14.80	4.66	8.8342	9.1491
65	PSW_C2	17.7	15.01	5.11	11.0600	11.1316
66	PSW_B2	16.1	15.03	4.61	8.8463	8.9073
67	PSW_D2	16.7	15.66	4.46	9.6881	9.9645
68	PSW_A1	16.5	15.46	4.50	8.8197	8.8573
69	PSW_C1	15.3	15.02	4.40	8.9309	9.0413

70	PSW_B1	16.0	14.98	4.65	8.6742	8.6042
71	PSW_DP1	…	15.14	…	8.5778	8.7195
72	PSW_D1	15.6	15.25	4.39	8.7030	8.6364
73	PSW_F12	16.6	14.68	5.13	9.4808	9.5194
74	PSW_J11	16.9	14.58	5.34	9.1845	9.0698
75	PSW_E12	15.9	15.07	4.65	8.8863	8.9129
76	PSW_H12	15.9	14.75	4.90	8.9737	8.7785
77	PSW_G12	15.0	14.44	4.87	8.9646	8.5882
78	PSW_F13	16.3	14.96	5.01	9.2463	9.4645
79	PSW_E13	15.7	15.16	4.54	8.6413	9.0661
80	PSW_J12	16.1	15.04	4.79	8.9203	9.0849
81	PSW_H13	16.7	15.18	4.93	8.8986	9.2446
82	**PSW_G13**	16.5	14.92	5.02	8.8848	9.0857
83	PSW_F14	16.5	15.19	4.78	8.9281	9.3866
84	PSW_E14	18.2	15.33	5.11	10.3628	9.8874
85	PSW_J13	15.5	14.75	4.78	9.3488	8.8043
86	PSW_H14	15.8	14.58	5.04	8.7598	8.7677
87	PSW_G14	16.9	14.93	5.10	10.1120	9.1013
88	PSW_J14	16.8	15.19	4.83	9.9392	9.5662
89	PSW_F15	15.7	15.03	4.64	8.8956	9.0105
90	PSW_H15	16.8	14.95	5.04	9.2221	9.4798
91	PSW_J15	16.4	14.71	5.01	9.2750	8.7415
92	PSW_G15	16.4	15.02	4.81	8.9267	8.9098
93	PSW_H16	16.6	…	…	9.0663	8.9192
94	**PSW_DP2**	…	14.96	…	8.6406	8.8259
95	PSW_F16	16.4	15.00	4.76	8.5217	9.0532
96	PSW_E15	15.6	14.87	4.64	8.8158	8.7848
97	PSW_D11	15.4	15.17	4.36	8.3923	8.6768
98	**PSW_A10**	…	15.01	…	0.0000	0.0000
99	PSW_E10	15.9	15.59	4.37	8.5676	8.3786
100	PSW_C10	16.5	15.30	4.68	8.8479	9.1018
101	PSW_B10	16.1	14.77	5.06	9.2584	9.0229
102	PSW_D10	15.3	14.74	4.65	8.4202	8.4726
103	PSW_A9	15.7	15.09	4.55	8.5947	8.5637
104	PSW_E9	15.7	…	…	8.3290	8.3469
105	PSW_C9	16.7	15.04	4.99	8.7889	10.0501
106	PSW_B9	17.7	15.15	5.12	10.5593	10.1350
107	PSW_D9	17.1	15.06	4.99	8.6304	8.5674
108	**PSW_A8**	15.2	15.05	4.45	8.6805	8.7726
109	PSW_C8	16.4	14.77	4.98	9.0868	9.0773

110	PSW_E8	16.0	15.36	4.49	8.6475	8.5460
111	PSW_D8	16.3	15.86	4.48	8.5308	8.4654
112	PSW_B8	15.7	15.19	4.56	9.1206	8.5503
113	PSW_C7	17.2	15.39	4.80	8.8960	8.7285
114	PSW_E7	15.4	15.11	4.46	8.8269	8.9297
115	PSW_A7	18.6	15.14	5.37	9.8279	9.2626
116	PSW_D7	16.4	14.86	4.94	8.6499	8.8837
117	PSW_B7	16.2	15.15	4.66	8.7210	8.8954
118	PSW_C6	16.0	15.63	4.35	8.3923	8.4543
119	PSW_E6	14.9	14.55	4.66	8.4639	8.5161
120	PSW_A6	15.7	15.06	4.65	8.5608	8.3189
121	PSW_G5	15.9	14.90	4.74	8.7881	8.8514
122	PSW_H6	16.9	15.03	4.97	8.7595	9.2343
123	**PSW_J6**	15.4	14.68	4.72	8.2611	8.2337
124	PSW_F6	16.2	15.14	4.71	8.9256	8.3086
125	PSW_G6	16.0	15.00	4.71	8.6950	8.5529
126	PSW_H7	15.4	14.86	4.61	8.6630	8.4827
127	PSW_F7	14.6	15.05	4.26	8.3517	8.4654
128	**PSW_J7**	857.0	…	…	52.0273	22.0472
129	PSW_G7	16.0	14.96	4.72	8.7456	8.9813
130	PSW_H8	15.4	15.00	4.61	8.6923	8.5501
131	**PSW_F8**	…	15.43	…	6.6267	6.6958
132	**PSW_G8**	…	15.12	…	0.0000	0.0000
133	PSW_J8	16.4	15.12	4.84	8.3825	8.4899
134	**PSW_F9**	15.7	15.16	4.56	16.3267	16.3854
135	**PSW_H9**	15.0	15.12	4.38	8.3610	8.4164
136	PSW_G9	15.5	…	…	8.6297	9.0497
137	PSW_J9	15.0	15.02	4.44	8.1463	8.1878
138	PSW_F10	15.8	14.74	4.84	8.8443	8.8966
139	PSW_H10	16.9	15.09	4.96	9.4236	9.2787
140	PSW_G10	16.5	15.02	4.91	9.4913	9.7976
141	**PSW_F11**	19.5	14.86	5.95	11.8097	11.5273
142	PSW_J10	17.3	14.94	5.13	9.5864	9.3378
143	PSW_H11	15.7	14.56	4.98	8.4829	8.5080
144	**PSW_G11**	696.0	14.96	210.33	8.2430	8.1811
145	PLW_R1	15.7	…	…	8.9361	0.0000
146	PLW_A8	17.3	17.11	4.00	0.0000	8.1932
147	PLW_A7	16.5	15.88	4.32	8.4943	9.0376
148	**PLW_A6**	20.8	15.99	5.39	9.4022	8.9958
149	PLW_A9	17.3	16.73	4.12	8.9721	8.5627

150	**PLW_C9**	16.7	16.07	4.28	8.4384	8.4476
151	PLW_B8	17.3	16.86	4.13	8.5457	8.7912
152	PLW_B7	17.4	16.21	4.43	8.8749	8.8271
153	PLW_C7	16.6	16.37	4.14	8.7485	9.0007
154	PLW_B5	19.2	16.26	4.86	8.7954	11.0786
155	PLW_B6	15.6	15.38	4.36	10.9229	8.6635
156	PLW_A5	18.8	16.39	4.73	8.5876	9.4448
157	PLW_T1	15.2	…	…	9.6082	8.6608
158	**PLW_B4**	17.7	16.17	4.55	8.7005	9.2661
159	PLW_C4	17.0	16.21	4.36	9.4531	9.3787
160	PLW_B3	15.8	15.59	4.42	8.8164	8.7259
161	PLW_C2	16.7	16.39	4.33	8.5252	8.6849
162	PLW_B2	17.4	15.67	4.91	8.3855	8.6495
163	PLW_B1	18.1	16.15	4.84	8.5765	9.1731
164	PLW_A3	18.6	16.23	4.84	8.6738	9.1183
165	PLW_A4	17.3	15.95	4.64	9.0242	8.9951
166	PLW_A1	16.7	16.23	4.44	8.7833	8.7482
167	**PLW_DP1**	…	16.34	…	9.0396	8.7124
168	**PLW_A2**	20.4	16.22	5.35	8.5153	14.5359
169	PLW_E1	17.1	16.07	4.47	9.0290	8.5350
170	**PLW_E2**	16.1	16.24	4.20	8.4386	8.3823
171	PLW_E3	16.0	15.59	4.40	8.4268	8.5833
172	PLW_E4	17.3	16.17	4.43	8.1790	8.6101
173	PLW_D1	19.4	16.20	5.09	9.6922	10.0156
174	PLW_D2	16.1	16.08	4.29	8.5001	8.2830
175	PLW_D3	17.2	16.21	4.46	8.9093	9.3175
176	PLW_D4	16.2	15.65	4.40	8.3103	8.3793
177	PLW_C1	15.4	15.52	4.35	8.4958	8.5710
178	PLW_C3	19.6	16.22	5.13	9.4547	9.3352
179	PLW_C5	15.5	15.47	4.23	8.6350	8.8265
180	**PLW_T2**	15.7	…	…	8.6568	9.1160
181	PLW_E5	16.8	14.99	4.82	11.0944	11.0876
182	PLW_C6	15.6	14.97	4.45	8.6111	8.4039
183	PLW_C8	16.3	15.94	4.19	8.2746	8.5743
184	PLW_D5	16.1	16.02	4.12	8.7686	8.3307
185	PLW_D6	15.9	15.82	4.18	8.1412	8.1580
186	PLW_D7	16.8	16.25	4.20	8.9578	8.4860
187	PLW_D8	19.1	15.50	5.20	9.9250	9.6000
188	PLW_E7	17.1	16.34	4.23	8.9426	9.0211
189	**PLW_E6**	20.9	16.19	5.27	9.7323	9.4626

190	PLW_E8	16.3	15.98	4.14	8.6033	8.7627
191	PLW_DP2	…	16.27	…	8.0723	8.4167
192	PLW_E9	16.7	16.21	4.18	8.5109	8.7085
193	**PMW_A13**	15.1	14.44	4.16	8.8179	8.6374
194	PMW_T1	15.1	…	…	8.1077	8.0865
195	PMW_B12	16.2	14.72	4.81	8.4657	8.9386
196	PMW_C13	15.4	14.46	4.78	8.4513	8.5024
197	PMW_A12	15.3	14.72	4.55	8.3312	8.3285
198	PMW_D12	15.3	15.06	4.40	8.6282	8.5489
199	PMW_C12	15.5	15.10	4.44	8.5625	8.6044
200	**PMW_B11**	27.3	14.73	8.21	8.0899	8.3137
201	**PMW_A11**	17.5	14.87	5.18	9.6982	9.5994
202	PMW_E13	15.9	14.67	4.80	8.9416	9.2633
203	PMW_D11	14.2	14.47	4.46	7.9694	8.0876
204	PMW_C11	14.8	14.70	4.50	8.3421	8.4146
205	PMW_B10	15.3	15.51	4.17	8.5856	8.3008
206	PMW_A10	14.8	14.51	4.57	8.3911	8.5278
207	PMW_D10	15.8	14.83	4.68	8.8811	8.3324
208	PMW_B9	15.1	14.59	4.61	7.8589	8.2856
209	PMW_C10	15.6	14.81	4.65	8.0361	8.1214
210	**PMW_C9**	15.1	14.34	4.78	8.4409	8.9699
211	PMW_A9	16.1	15.54	4.35	8.6523	8.2331
212	PMW_B8	16.8	15.03	4.81	8.7485	8.5771
213	**PMW_A8**	18.7	14.44	5.73	11.1799	11.2529
214	PMW_D8	16.1	15.23	4.50	8.5225	8.9200
215	**PMW_C8**	…	14.44	…	0.0000	0.0000
216	PMW_B7	14.6	14.36	4.54	8.1608	8.4945
217	PMW_R1	14.6	…	…	0.0000	0.0000
218	PMW_G1	16.3	14.49	5.37	8.4955	8.7523
219	**PMW_T2**	…	…	…	0.0000	0.0000
220	PMW_E1	16.0	14.46	5.24	8.1666	8.5659
221	PMW_D1	16.9	14.25	5.76	9.8522	9.6303
222	PMW_F1	20.5	14.49	6.76	10.1690	9.8196
223	PMW_E2	15.1	14.57	4.87	8.7861	8.5663
224	PMW_G2	16.0	14.41	5.25	8.1499	8.1503
225	**PMW_F2**	16.3	14.57	5.31	9.2834	8.9726
226	PMW_G3	16.1	14.55	5.20	8.2204	8.5311
227	PMW_E3	14.9	14.51	4.82	8.1292	8.5966
228	PMW_D3	16.4	14.96	5.02	8.1835	8.7405
229	PMW_F3	15.8	14.74	4.97	8.5797	8.9601

230	PMW_G4	17.1	14.86	5.24	8.0918	8.6041
231	**PMW_E4**	25.0	15.07	7.46	8.9360	8.9870
232	PMW_F4	14.9	14.44	4.81	8.1222	8.1606
233	**PMW_E5**	23.7	14.38	7.63	8.3407	7.9542
234	PMW_D5	17.1	14.71	5.32	8.3662	9.2216
235	**PMW_F5**	25.8	14.63	8.05	9.4163	9.0715
236	PMW_G5	15.8	14.94	4.73	9.3086	8.6917
237	PMW_E6	15.5	14.32	5.09	8.0133	8.5052
238	**PMW_G6**	34.3	14.60	10.67	8.9500	8.5893
239	**PMW_F6**	19.2	14.94	5.68	8.7028	8.6696
240	**PMW_G7**	17.5	14.62	5.37	8.3957	8.5351
241	PMW_F10	16.0	14.79	4.89	9.3811	9.5862
242	PMW_E11	15.5	14.91	4.66	8.3868	8.5525
243	**PMW_G11**	…	14.57	…	6.1495	6.7925
244	PMW_F11	15.3	14.56	4.79	8.3095	8.4400
245	PMW_E12	15.2	15.65	4.15	8.6542	8.3594
246	PMW_G12	15.6	14.70	4.74	8.8632	8.4064
247	PMW_F12	17.2	15.10	5.40	8.4422	8.1047
248	PMW_G13	18.4	14.66	5.70	9.5776	9.4443
249	PMW_DP2	…	15.07	…	8.3820	8.3061
250	PMW_E7	16.4	14.63	5.02	8.7663	8.3745
251	PMW_D7	19.8	14.33	6.30	10.2493	10.9014
252	**PMW_F7**	…	14.67	…	9.6686	9.6468
253	PMW_E8	14.6	14.42	4.62	8.6594	8.5615
254	PMW_G8	15.6	14.76	4.64	8.6640	8.2712
255	PMW_F8	14.9	14.88	4.41	8.5583	8.3531
256	PMW_E9	15.9	15.47	4.36	8.6076	8.1490
257	**PMW_G9**	…	14.81	…	6.7168	6.5475
258	**PMW_D9**	16.1	15.35	4.54	9.2268	8.9915
259	PMW_F9	15.3	14.72	4.69	8.8328	8.4356
260	PMW_E10	16.6	14.79	5.06	8.6688	8.6769
261	PMW_G10	15.8	14.21	5.19	8.1140	8.2281
262	PMW_C4	15.8	14.99	4.56	8.5802	8.5888
263	PMW_B3	15.6	15.01	4.50	8.5117	8.4728
264	PMW_C3	15.6	15.63	4.24	8.5505	8.0738
265	PMW_B2	18.7	14.85	5.53	10.4664	10.8088
266	PMW_D2	19.3	15.03	5.59	11.1044	10.7341
267	PMW_A3	15.3	14.93	4.43	8.5085	8.4099
268	PMW_A2	16.2	14.84	4.71	8.7778	8.7252
269	PMW_C2	15.8	15.05	4.53	8.0671	8.4538

270	**PMW_B1**	18.2	15.07	5.18	9.3204	9.5362
271	PMW_A1	15.6	14.55	4.75	9.1959	8.8601
272	**PMW_DP1**	…	15.01	…	10.4557	10.2632
273	PMW_C1	16.2	15.42	4.39	8.6298	8.8269
274	PMW_A7	15.4	14.88	4.35	9.1501	8.7087
275	PMW_A6	18.5	14.73	5.41	9.4780	10.0970
276	**PMW_B6**	…	14.75	…	6.5143	6.3947
277	PMW_C7	16.3	14.63	4.80	8.8354	9.0802
278	PMW_A5	15.7	15.00	4.45	8.5082	8.5718
279	PMW_B5	17.3	14.84	4.99	9.1756	8.9660
280	PMW_C6	16.0	15.06	4.50	8.6025	8.4893
281	**PMW_D6**	26.9	14.92	7.64	15.4015	15.7425
282	PMW_B4	17.8	15.13	4.97	9.3710	9.2738
283	PMW_C5	15.1	15.58	4.02	8.2845	8.2884
284	PMW_D4	15.7	15.49	4.24	8.3046	8.2944
285	PMW_A4	15.1	14.80	4.38	7.7871	8.3088
286	PMW_P1	10.5	…	…	6.6350	6.4049
287	PMW_P2	10.5	…	…	6.9039	6.7731
288	PMW_P3	10.2	…	…	6.3450	6.2302

Table 7-7-2: Similar to Table 7-1: Spectrometer channel noises from a noise measurement with (T_subk, f_bias, V_bias) = (0.286K, 212.29Hz, 40.1mV), which is near the optimal bias setting for the spectrometer arrays, of OBSID = 3001223E.

No.	Channel	Observed Noise (nV/sq(Hz))	Model Noise (nV/sq(Hz))	Observed NEP (1E-17) W/sq(Hz)	Warm Noise PFM5	
					prime (nV/sq(Hz))	redundant (nV/sq(Hz))
1	SSW_R1	17.6	...	...	0.0000	0.0000
2	SSW_A4	15.5	15.15	6.09	8.1441	8.3182
3	**SSW_A3**	21.2	15.39	8.20	9.0452	8.9635
4	**SSW_A2**	16.2	15.09	6.34	7.5645	7.3844
5	SSW_A1	15.9	15.65	5.95	7.6600	7.6280
6	SSW_DP1	15.0	14.46	6.43	7.4293	7.4474
7	SSW_B3	17.9	15.71	6.63	8.6287	8.8059
8	SSW_B2	16.1	15.49	6.06	8.0386	7.8326
9	SSW_B1	18.0	15.12	7.10	8.4358	8.2602
10	SSW_C3	16.5	15.13	6.42	7.6198	7.6662
11	SSW_C2	15.6	15.25	6.03	7.9566	7.7544
12	SSW_C1	16.2	15.72	6.01	7.8927	7.3650
13	SSW_D3	15.2	15.09	5.93	8.6230	7.9507

14	SSW_D2	17.7	15.14	6.95	9.5511	9.4392
15	SSW_D1	16.5	15.87	6.06	7.4597	7.2493
16	**SSW_E3**	16.0	15.66	5.98	7.8611	7.8818
17	SSW_E2	15.7	15.88	5.72	7.5834	7.5864
18	SSW_E1	15.9	15.67	5.89	7.8026	7.9161
19	SSW_F3	18.1	17.24	5.89	7.7927	7.6737
20	SSW_F2	16.7	18.11	5.06	7.2745	7.0835
21	SSW_F1	16.3	14.99	6.41	8.8260	8.8128
22	SSW_G1	18.6	19.01	5.24	7.4286	7.5172
23	SSW_T1	16.2	...	…	7.6227	7.7341
24	SSW_G2	16.3	15.45	6.15	7.3351	7.3947
25	SSW_E5	17.7	16.24	6.35	7.7890	7.5968
26	SSW_E4	15.9	14.87	6.47	7.4049	7.3216
27	**SSW_D7**	16.5	15.14	6.57	7.4989	7.6849
28	SSW_D6	17.1	...	...	8.0193	8.0036
29	**SSW_D5**	…	...	...	0.0000	0.0000
30	SSW_D4	15.7	15.03	6.20	7.3080	7.3573
31	SSW_C6	17.3	15.15	6.85	9.2333	9.0981
32	SSW_C5	18.1	15.97	6.63	7.9080	7.6862
33	SSW_C4	16.6	15.14	6.64	7.5383	7.5611
34	SSW_B5	17.7	17.31	5.75	7.3269	7.4011
35	SSW_B4	17.4	15.84	6.44	7.4817	7.8710
36	SSW_T2	17.0	...	2.92	7.3515	7.2358
37	SSW_G3	18.1	14.81	7.31	7.3658	7.3429
38	SSW_G4	15.1	15.28	5.76	8.0111	8.1290
39	SSW_DP2	17.2	14.59	7.38	7.6032	7.7245
40	SSW_F5	18.7	19.21	5.30	7.1984	7.3554
41	**SSW_F4**	314.0	15.07	118.24	13.0132	11.5462
42	SSW_E6	16.1	14.78	6.61	7.7277	7.8335
43	NC1	18.5	...	...	13.4607	13.3599
44	NC2	18.4	...	...	13.2343	13.1382
45	NC3	20.6	...	...	14.3856	14.3679
46	NC4	18.8	...	...	13.3999	13.4202
47	NC5	17.9	...	...	13.5203	13.4599
48	NC6	19.0	...	...	13.2275	13.1839
49	SLW_R1	13.5	...	...	0.0000	0.0000
50	SLW_T1	20.6	...	2.48	10.7427	10.7892
51	**SLW_C1**	17.9	15.05	6.77	8.1342	7.8258
52	SLW_DP1	19.1	15.03	7.48	7.4660	8.0016
53	SLW_B1	17.9	16.22	6.00	7.4173	7.8226

54	SLW_D1	18.1	15.44	6.55	9.8710	9.9151
55	SLW_E1	17.6	15.43	6.52	7.7925	7.9087
56	SLW_A1	17.7	15.20	6.46	8.0562	8.0186
57	**SLW_C2**	…	15.93	…	10.3507	10.5247
58	**SLW_D2**	19.2	18.24	5.43	7.7398	7.6882
59	SLW_B2	17.9	15.90	6.00	8.4100	8.2306
60	**SLW_E2**	19.9	17.68	5.91	7.8538	7.7579
61	SLW_A2	18.1	15.90	6.20	7.9873	8.1247
62	SLW_C3	19.6	17.34	5.88	7.6073	7.6547
63	SLW_D3	17.1	15.79	5.92	8.3981	7.9526
64	**SLW_B3**	…	17.26	…	10.4931	10.5727
65	SLW_E3	17.3	15.73	6.26	7.9480	7.7723
66	SLW_C4	16.8	15.87	5.72	7.5344	7.4854
67	**SLW_DP2**	…	...	...	0.0000	0.0000
68	SLW_D4	19.6	19.68	5.04	7.7128	7.7341
69	SLW_C5	17.2	16.14	5.86	7.8348	7.3560
70	SLW_B4	16.8	15.78	5.77	7.2095	7.3315
71	**SLW_A3**	16.3	15.49	5.82	7.2734	7.7989
72	**SLW_T2**	19.1	...	…	11.6457	11.4591